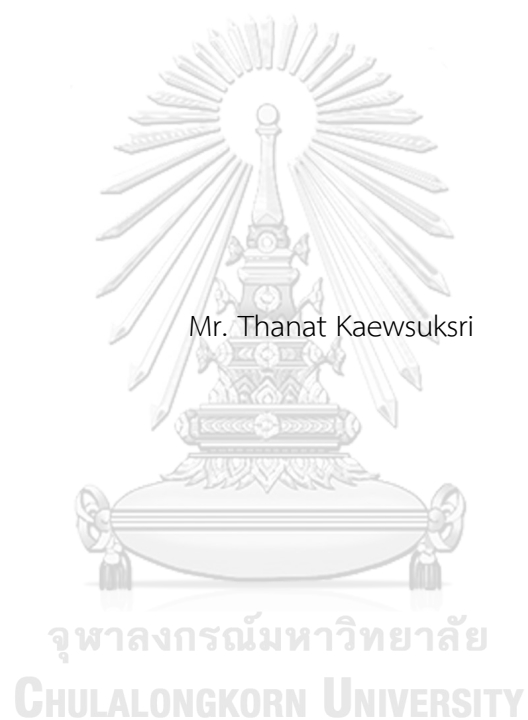


Accuracy of Small-Field High Energy Photon Using Plastic Scintillation Detector in  
Heterogenous Media Compared with Model-Based Algorithm Calculation



A Thesis Submitted in Partial Fulfillment of the Requirements  
for the Degree of Master of Science in Medical Physics

Department of Radiology

FACULTY OF MEDICINE

Chulalongkorn University

Academic Year 2022

Copyright of Chulalongkorn University

การประเมินความถูกต้องของอัลกอริทึมที่ใช้ในการวางแผนการรักษาด้วยลำรังสีโฟตอนพลังงานสูง  
ขนาดเล็กภายในตัวกลางความหนาแน่นไม่คงที่เปรียบเทียบกับค่าที่วัดได้โดยซินทิลเลเตอร์พลาสติก



วิทยานิพนธ์นี้เป็นส่วนหนึ่งของการศึกษาตามหลักสูตรปริญญาวิทยาศาสตรมหาบัณฑิต  
สาขาวิชาฟิสิกส์การแพทย์ ภาควิชารังสีวิทยา  
คณะแพทยศาสตร์ จุฬาลงกรณ์มหาวิทยาลัย  
ปีการศึกษา 2565  
ลิขสิทธิ์ของจุฬาลงกรณ์มหาวิทยาลัย

Thesis Title                      Accuracy of Small-Field High Energy Photon Using  
Plastic Scintillation Detector in Heterogenous Media  
Compared with Model-Based Algorithm Calculation

By                                      Mr. Thanat Kaewsuksri

Field of Study                      Medical Physics

Thesis Advisor                      Assistant Professor Taweap Sanghangthum, Ph.D.

---

Accepted by the FACULTY OF MEDICINE, Chulalongkorn University in Partial  
Fulfillment of the Requirement for the Master of Science

----- Dean of the FACULTY OF MEDICINE  
(Associate Professor Chanchai Sittipunt, M.D.)

THESIS COMMITTEE

----- Chairman  
(Sornjarod Oonsiri, Ph.D.)

----- Thesis Advisor  
(Assistant Professor Taweap Sanghangthum, Ph.D.)

----- External Examiner  
(Professor Franco Milano, Ph.D.)

จุฬาลงกรณ์มหาวิทยาลัย  
CHULALONGKORN UNIVERSITY

ธนัท แก้วสุขศรี : การประเมินความถูกต้องของอัลกอริทึมที่ใช้ในการวางแผนการรักษาด้วยลำรังสีโฟตอนพลังงานสูงขนาดเล็กภายในตัวกลางความหนาแน่นไม่คงที่เปรียบเทียบกับค่าที่วัดได้โดยซินทิลเลเตอร์พลาสติก . (Accuracy of Small-Field High Energy Photon Using Plastic Scintillation Detector in Heterogenous Media Compared with Model-Based Algorithm Calculation) อ.ที่ปรึกษาหลัก: ผศ. ดร. ทวีป แสงแห่งธรรม

โฟตอนพลังงานสูงขนาดเล็กถูกนำมาใช้ในงานรักษาด้วยเทคนิคต่าง ๆ เช่นการฉายรังสีร่วมพิภัก (Stereotactic body radiotherapy; SBRT) เนื่องจากลดปริมาณรังสีไปยังเนื้อเยื่อปกติได้ ถึงอย่างไรก็ตามการวัดปริมาณรังสีโฟตอนขนาดเล็กยังคงมีความคาดเคลื่อนสูงโดยเฉพาะอย่างยิ่งภายในตัวกลางที่ความหนาแน่นไม่คงที่ การศึกษานี้มีวัตถุประสงค์ในการประเมินความถูกต้องของหัววัดรังสีแบบซินทิลเลเตอร์พลาสติก (Plastic scintillation detector; PSD) โดยเปรียบเทียบกับค่าคำนวณของอัลกอริทึม การศึกษานี้ประกอบไปด้วยการศึกษาคุณลักษณะเฉพาะของ W2-PSD การเปรียบเทียบปริมาณรังสีตามระยะลึก (Percentage depth dose; PDD) ภายในตัวกลางที่เป็นอากาศ (สไตโรโฟม) เนื้อเยื่อปอด (ไม้คอร์ก) และอะลูมิเนียม การศึกษาแสดงให้เห็นว่า W2-PSD มีความสามารถในการวัดซ้ำ (Repeatability) ความเป็นเชิงเส้นของปริมาณรังสีกับสัญญาณที่วัดได้ (Linearity) ที่ดีและยังขึ้นอัตราปริมาณรังสี (Repetition rate) และพลังงาน (Energy dependence) เล็กน้อย โดยมีค่า deviation สูงสุดไม่เกิน 1% สำหรับการศึกษ PDD พบว่าปริมาณรังสีมีค่าลดลงภายในตัวกลางอากาศและเนื้อเยื่อปอดก่อนที่จะสูงขึ้นเมื่อเข้าสู่ตัวกลางที่เป็นน้ำ ซึ่งจะตรงข้ามกับกรณีในตัวกลางเป็นอะลูมิเนียมที่ปริมาณรังสีจะมีค่าสูงขึ้นก่อนเข้าสู่ตัวกลางที่เป็นอะลูมิเนียมหลังจากนั้นจึงค่อยลดลง โดยปริมาณรังสีที่วัดได้กับการคำนวณของอัลกอริทึมจะมีความแตกต่างกันมากขึ้นเมื่อพลังงานของโฟตอนสูงขึ้น ขนาดของรังสีและความหนาแน่นของตัวกลางมีค่าลดลง สำหรับการเปรียบเทียบปริมาณรังสีทางคลินิกในผู้ป่วยที่ได้รับการรักษาด้วย SBRT พบว่าความแตกต่างของปริมาณรังสีที่วัดได้กับการคำนวณของอัลกอริทึมมีค่าไม่เกิน 5% ดังนั้นการใช้ W2-PSD สามารถนำมาใช้ในการวัดปริมาณรังสีโฟตอนขนาดเล็กภายในตัวกลางความหนาแน่นไม่คงที่ตามข้อบังคับของ IAEA TRS 430

สาขาวิชา ฟิสิกส์การแพทย์  
ปีการศึกษา 2565

ลายมือชื่อนิสิต .....  
ลายมือชื่อ อ.ที่ปรึกษาหลัก .....

# # 6470028030 : MAJOR MEDICAL PHYSICS

KEYWORD: Small field, Plastic scintillation detector, Heterogeneous media

Thanat Kaewsuksri : Accuracy of Small-Field High Energy Photon Using Plastic Scintillation Detector in Heterogenous Media Compared with Model-Based Algorithm Calculation. Advisor: Asst. Prof. TAWEAP SANGHANGTHUM, Ph.D.

Some radiotherapy techniques such as stereotactic body radiotherapy (SBRT) has the challenges in small field dosimetry in heterogenous media. This study aims at evaluating the accuracy of W2 plastic scintillation detector (PSD) compared with the calculation from algorithms for small-field high energy photon in heterogenous media. The characteristics of W2-PSD were studied. The percentage depth dose (PDD) of 6 FFF and 10 FFF with various field sizes ranging from 1x1 to 4x4 cm<sup>2</sup> were measured in solid water phantom with low-density inhomogeneities slabs of air (Styrofoam) and lung (cork) and high-density inhomogeneity slab of aluminum. The characteristics of W2 plastic scintillator were very good in terms of repeatability and linearity. The maximum deviation of repetition rate and energy dependence were within 1%. The PDD results showed the same trend in both air and lung heterogeneity which presented the dose drop in heterogeneous media region and re-buildup after that. On the contrary, in aluminum heterogeneity the dose increased at upper interface. The large difference of PDD curve inside heterogeneous media was presented with higher energy, smaller field size and lower density medium. From the SBRT clinical application results, the differences between measured and calculated doses were within 5%. Hence, the W2-PSD is possible to be used for small-field dosimetry in heterogeneous media according to IAEA TRS 430.

Field of Study: Medical Physics

Student's Signature .....

Academic Year: 2022

Advisor's Signature .....

## ACKNOWLEDGEMENTS

Foremost, I would like to express my very sincere appreciation and gratitude to my advisor, Assistant Professor Taweap Sanghangthum, Ph. D., Division of Radiation Oncology, Department of Radiology, Faculty of Medicine, Chulalongkorn University for his continuous support and guidance on my M.Sc. degree study and this research with kind suggestions and insightful comments. I would like to acknowledge with sincere thanks the kind support and guidance that I have received from Mr. Jaruek Kanphet, Division of Radiation Oncology, Department of Radiology, King Chulalongkorn Memorial Hospital. I would like to express my appreciation to Associate Professor Sivalee Suriyapee, Division of Radiation Oncology, Department of Radiology, Faculty of Medicine, Chulalongkorn University, for her teaching knowledge and kind comments.

I would like to thank my thesis committee: Dr. Sornjarod Oonsiri, Division of Radiation Oncology, Department of Radiology, Faculty of Medicine, Chulalongkorn University Chairman of my thesis committee, and Professor Franco Milano, Ph.D., University of Florence, Italy. External Examiner of the thesis defense for their encouragement and constructive comments.

I would like to express my thanks to all the lecturers, medicals physicist, and staff at the Medical Physics program for their knowledge and suggestion during my M.Sc. study. I would like to thank my colleague for their support and friendship.

Lastly, I would like to my family, for their love, support and encouragement through my life.

Thanat Kaewsuksri

## TABLE OF CONTENTS

	Page
ABSTRACT (THAI) .....	iii
ABSTRACT (ENGLISH) .....	iv
ACKNOWLEDGEMENTS .....	v
TABLE OF CONTENTS .....	vi
LIST OF FIGURES.....	1
LIST OF TABLES.....	4
LIST OF ABBREVIATIONS.....	5
CHAPTER I INTRODUCTION .....	6
1.1 Background and rational.....	6
1.2 Objectives .....	7
CHAPTER II REVIEW OF RELATED LITERATURES.....	8
2.1 Theory.....	8
2.1.1 Definition of small fields .....	8
2.1.2 Lateral charged particle equilibrium range.....	9
2.1.3 General characteristics of detectors for small field relative dosimetry.....	10
2.1.4 Plastic scintillation detector (PSD) .....	11
2.1.5 Volumetric-modulated arc therapy .....	12
2.1.6 Stereotactic body radiation therapy.....	13
2.2 Reviews of related literatures.....	13
CHAPTER III RESEARCH METHODOLOGY .....	18
3.1 Research design.....	18

3.2 Research design model .....	18
3.2.1 W2 plastic scintillator characteristics in water .....	18
3.2.2 Percentage depth dose in heterogenous media .....	19
3.2.3 Clinical application in CIRS thorax phantom .....	19
3.3 Conceptual framework .....	20
3.4 Research questions .....	20
3.5 Materials .....	20
3.5.1 Varian TrueBeam™ linear accelerator .....	20
3.5.2 CT simulator .....	21
3.5.3 Exradin W2 plastic scintillator .....	22
3.5.4 Solid water slab phantom .....	23
3.5.5 Heterogeneous slab phantom .....	23
3.5.6 CIRS thorax phantom .....	24
3.5.7 Eclipse™ treatment planning system .....	25
3.6 Methods .....	25
3.6.1 Pre-irradiation: plastic scintillator calibration .....	26
3.6.1.1 Small field water tank calibration method .....	26
3.6.2 The W2 plastic scintillator characteristics in water .....	30
3.6.2.1 Short-term reproducibility .....	31
3.6.2.2 Linearity .....	31
3.6.2.3 Repetition rate response .....	31
3.6.2.4 Energy dependency .....	32
3.6.3 Percentage depth dose in heterogenous media .....	32
3.6.4 Clinical application in CIRS thorax phantom .....	34



3.7 Statistical analysis .....	36
3.8 Sample size determination .....	37
3.9 Outcome measurement.....	37
3.10 Benefit of research.....	38
3.11 Ethical consideration .....	38
CHAPTER IV RESULTS.....	39
4.1 W2 plastic scintillator characteristics in water.....	39
4.1.1 Short-term reproducibility.....	39
4.1.2 Linearity .....	40
4.1.3 Repetition rate response .....	40
4.1.4 Energy dependency .....	41
4.2 Percentage depth dose in heterogenous media .....	41
4.2.1 Air heterogeneous media.....	46
4.2.2 Lung heterogeneous media.....	46
4.2.3 Aluminum heterogeneous media .....	47
4.3 Clinical application in CIRS thorax.....	47
CHAPTER V DISCUSSION AND CONCLUSION.....	48
5.1 Discussion.....	48
5.1.1 W2 plastic scintillator characteristics in water .....	48
5.1.2 Percentage depth dose in heterogeneous media.....	48
5.1.3 Clinical application in CIRS thorax phantom .....	49
5.2 Conclusion .....	49
REFERENCES.....	51
APPENDIX .....	54

VITA.....57



จุฬาลงกรณ์มหาวิทยาลัย  
**CHULALONGKORN UNIVERSITY**

## LIST OF FIGURES

Figure 2.1	When the field size is reduced, it obstructs the source and limits the photon fluence (left). As the field size is reduced, the penumbra from opposing jaws overlap and the dose drop at the center of the field. As a result, the fullwidth haft maximum of the dose profile is no longer equal to the collimator setting (right)	9
Figure 2.2	Energy levels of organic molecules inside plastic scintillation detector	12
Figure 2.3	Sample setup showing scintillator plate reserved to measure the dose at entrance junction of heterogenous slab. The detector is shown as a small circle and the arrow shows the beam entry point on the phantom	14
Figure 2.4	The central axis depth dose (CADD) curves of measured and four algorithms for lung heterogeneity in 6 MV far to Dmax setup for field size 1x1 cm <sup>2</sup> . Lung heterogeneity region is shown in shaded area	15
Figure 2.5	Curves of %NRMSD respect to W2 plastic scintillator measurement for every field size in two different lung heterogeneity setups for 6 MV photon beam	16
Figure 2.6	Geometrical layout of phantoms. Setting A on the left; and setting B in the middle; sectors used in the 2D gamma analysis for setting A on the right	17
Figure 3.1	Research design model of W2 plastic scintillator characteristics in water	18
Figure 3.2	Research design model of percentage depth dose in heterogeneous media	19
Figure 3.3	Research design model of clinical application in CIRS thorax phantom	19
Figure 3.4	Conceptual framework	20
Figure 3.5	Varian TrueBeam <sup>TM</sup> linear accelerator	21

Figure 3.6	Siemens SOMATOM CT simulator .....	22
Figure 3.7	Exradin W2 plastic scintillation detector (W2-PSD ) .....	23
Figure 3.8	Solid water slab phantom .....	23
Figure 3.9	Heterogeneous slab phantom, air (top-left), lung (top-right) and aluminum (bottom) .....	24
Figure 3.10	CIRS thorax phantom .....	25
Figure 3.11	Maximum configuration setup .....	26
Figure 3.12	Minimum configuration setup .....	27
Figure 3.13	The example of W2 plastic scintillator system web-based interface for the point dose measurement .....	29
Figure 3.14	The example of W2 plastic scintillator system web-based interface in the calibration process .....	30
Figure 3.15	Heterogeneous phantom diagram .....	33
Figure 3.16	Heterogeneous phantom measurement setup .....	34
Figure 3.17	CIRS thorax phantom scanning .....	35
Figure 3.18	Calculated dose inside CIRS thorax phantom .....	35
Figure 3.19	CIRS thorax phantom measurement setup .....	36
Figure 4.1	Plotted curve of measured dose and monitor unit .....	40
Figure 4.2	The graph of repetition rate response .....	40
Figure 4.3	The percentage depth dose curve of 6 FFF with different field sizes in air heterogeneous media .....	42
Figure 4.4	The percentage depth dose curve of 10 FFF with different field sizes in air heterogeneous media .....	42
Figure 4.5	The percentage depth dose curve of 6 FFF with different field sizes in lung heterogeneous media .....	43
Figure 4.6	The percentage depth dose curve of 10 FFF with different field sizes in lung heterogeneous media .....	43
Figure 4.7	The percentage depth dose curve of 6 FFF with different field sizes in aluminum heterogeneous media .....	44
Figure 4.8	The percentage depth dose curve of 10 FFF with different field sizes in aluminum heterogeneous media .....	44

Figure 4.9	The plotted curves of %NRMSD of W2 plastic scintillator and AAA respect to Acuros for every field size in air heterogeneous media at two different energies .....	45
Figure 4.10	The plotted curves of %NRMSD of W2 plastic scintillator and AAA respect to Acuros for every field size in lung heterogeneous media at two different energies .....	46
Figure 4.11	The plotted curves of %NRMSD of W2 plastic scintillator and AAA respect to Acuros for every field size in aluminum heterogeneous media at two different energies .....	46



## LIST OF TABLES

Table 2.1	Characteristics of suitable detectors for relative dosimetry in small fields .....	10
Table 4.1	The result of W2 plastic scintillator short-term reproducibility .....	39
Table 4.2	The result of W2 plastic scintillator energy dependency .....	41
Table 4.3	The percentage difference between measured and calculated dose in CIRS thorax phantom .....	48



## LIST OF ABBREVIATIONS

Abbreviations	Terms
AAA	Analytical anisotropic algorithm
AXB	Acuros XB algorithm
CADD	Central axis depth dose
CLR	Cerenkov light ratio
$D_{\max}$	Depth of maximum dose
FFF	Flattening filter free
IMRT	Intensity modulated radiotherapy
LBTE	Linear Boltzmann transport equation
LCPE	Lateral charged particle equilibrium
MLC	Multileaf collimator
MU	Monitor unit
%NRMSD	Percentage normalized root mean squared deviation
PDD	Percentage depth dose
PSD	Plastic scintillation detector
$r_{LCPE}$	Lateral charged particle equilibrium range
RMSD	Root mean square deviation
SBRT	Stereotactic body radiotherapy
SD	Standard deviation
SP	Superposition algorithm
SRS	Stereotactic radiosurgery
SSD	Source to surface distance
$TPR_{20,10}(10)$	Tissue phantom ratio in water at the depths of 20 and 10 g/cm <sup>2</sup> , for field size of 10 cm x 10 cm defined at an SDD of 100 cm
TPS	Treatment planning system
VMAT	Volumetric modulated arc therapy
WFF	With flattening filter
XVMC	X-ray Voxel Monte Carlo

## CHAPTER I

### INTRODUCTION

#### 1.1 Background and rational

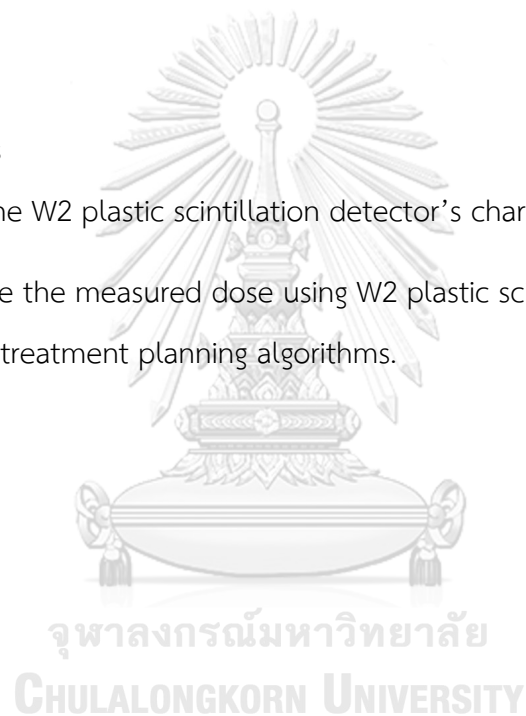
Radiotherapy is one of the most common cancer treatments that use high radiation doses to kill cancer cells. Many specific radiotherapy techniques including stereotactic radiosurgery (SRS) and stereotactic body radiotherapy (SBRT) involve small field to deliver high conformal dose to small targets while minimizing damage to healthy surrounding organs. However, the dosimetry in small field has difficulty measuring by dosimeter or calculating by treatment planning system (TPS) due to the lack of lateral charged particle equilibrium (LCPE) when the field size is smaller than the range of secondary electrons,<sup>(1)</sup> primary beam source occlusion, and volume averaging effect from large detector. Moreover, the dosimetry in heterogeneous such as air or lung faces a large uncertainty because of the perturbation in electron density of the media. The plastic scintillation detector is the one of recommended dosimeters used for small field dosimetry in water because it has minimal sensitive volume and water-equivalent density when compared to small sensitive volume ionization chambers and diodes.<sup>(2-4)</sup> One of the latest versions of commercial plastic scintillation detector is W2 scintillator (Standard Imaging, Middleton, WI) which was launched in 2018. To calculate the dose, the Monte Carlo simulation is one of most reliable tools for dose calculation especially in conditions where measurement has difficulty to perform such as steep or gradient dose area, small radiation field and heterogeneity region. The Monte Carlo simulation applies any interactions that might occur during irradiation. It also provides more accurate dose distribution in heterogeneous media. The Monte Carlo simulations are mostly used as the gold standard for dose calculation in radiotherapy and compared with detector measurement and dose calculation algorithms. However, in clinical application, many treatment planning systems do not utilize the full scale of Monte Carlo simulation-based algorithms due to the problem of time consuming. This study is interested in Acuros XB algorithms which are implemented in Eclipse treatment planning system



(Varian Medical Systems, Palo Alto, USA). It belongs to the class of the linear Boltzmann transport equation (LBTE) is similar to those used in Monte Carlo methods that focus on the dose deposition in media.<sup>(20)</sup> The purposes of this study were to find the W2 plastic scintillator's characteristics in water and to compare the measured dose using plastic scintillator with the calculated dose from TPS algorithms. The comparisons were provided in terms of percentage depth dose (PDD) in air, lung and air heterogeneous media and in terms of point dose differences in SBRT clinical application.

## 1.2 Objectives

- 1.2.1 To study the W2 plastic scintillation detector's characteristics in water.
- 1.2.2 To compare the measured dose using W2 plastic scintillator to calculate the dose from treatment planning algorithms.



## CHAPTER II

### REVIEW OF RELATED LITERATURES

#### 2.1 Theory

##### 2.1.1 Definition of small fields

Small fields have been defined as those radiation fields that satisfy at least one of the following conditions:

- (a) Lateral charged particle equilibrium (LCPE) lost on the beam's axis.
- (b) Collimating devices partially occlude the primary photon source in the beam axis.
- (c) The detector size is larger or equal to the dimensions of the beam.

The characteristics (a) and (b) are beam-related conditions, while (c) is detector related condition.<sup>(5-8)</sup>

Loss of LCPE in photon beams occurs when the half width of the beam is smaller than the maximum range of secondary electrons that contribute to absorbed dose. The lack of LCPE is a problem for photon dosimetry using non-water equivalent dosimeter. A practical parameter that quantitatively determines when field sizes are small is the LCPE range ( $r_{LCPE}$ ). The  $r_{LCPE}$  is defined as the minimum radius of a circular photon field for which collision kerma equals to absorbed dose to water at the center of the circular field.<sup>(9)</sup>

For the collimating condition, partial photon beam blocked by collimators leads to decreasing in photon fluence along the central beam axis resulting in a reduction of beam output and the overlap regions of the opposing penumbras as shown in Figure 2.1.<sup>(6)</sup>

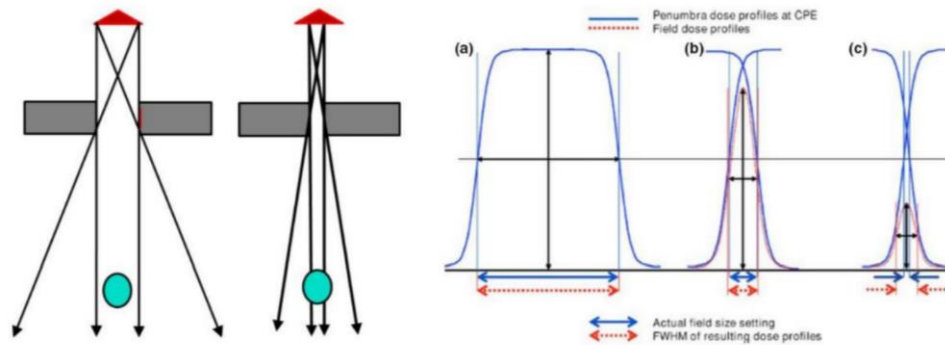


**Figure 2.1** When the field size is reduced, it obstructs the source and limits the photon fluence (left). As the field size is reduced, the penumbra from opposing jaws overlap and the dose drop at the center of the field. As a result, the fullwidth half maximum of the dose profile is no longer equal to the collimator setting (right).<sup>(5)</sup>

For the detector-related condition, the dosimeter generates a signal that is proportional to the absorbed dose over its sensitive volume. This signal is affected by the homogeneity of the absorbed dose over the detection volume called volume averaging effect. Beside this effect, the perturbation of the charged particle fluence due to the presence of a detector becomes large and difficult to predict. From IAEA TRS-430, small-field conditions can be assumed to establish when the external edge of the detector volume is at a distance from the field edge smaller than the  $r_{LCPE}$  in the medium. To avoid this condition in central axis measurements, the beam half width must be at least the length of  $r_{LCPE}$  plus a half of external detector volume length.<sup>(5)</sup>

### 2.1.2 Lateral charged particle equilibrium range

The lateral charged particle equilibrium range ( $r_{LCPE}$ ) is derived as the minimum radius of circular radiation field for which collision kerma equals to absorbed dose to water at the center of the field. Monte Carlo calculations have been performed for  $r_{LCPE}$  and expressed as a function of the conventional tissue phantom ratio quality index of  $TPR_{20,10}(10)$  as shown in equation (1).<sup>(5)(10)</sup>

$$r_{LCPE} = 8.369 \times TPR_{20,10}(10) - 4.382 \quad (1)$$

### 2.1.3 General characteristics of detectors for small field relative dosimetry

There is no ideal detector for small-field dosimetry. Users have to compromise the limitation of each detector such as volume averaging effect and substantial perturbations in the lack of LCPE. The general characteristics of suitable detectors for small field dosimetry are summarized in Table 2.1.<sup>(5)(6)</sup>

**Table 2.1** Characteristics of suitable detectors for relative small field dosimetry

Properties	Guidance
Stability	Short term detector response is better than 0.1% for a total accumulated absorbed dose up to hundreds of kGy from multiple exposures.
Dose linearity	Linearity is better than 0.1% over an absorbed dose in range of at least three orders of magnitude (e.g. 0.01-10 Gy).
Dose rate linearity	Detector signal is linear to better than 0.1% in the range of operation of the clinical linear accelerators.
Detector response energy	The useful energy range of the detectors for small field MV radiotherapy is from $^{60}\text{Co}$ to 10 MV.
Size of detector	The size of detector is such that the volume averaging correction is not larger than 5%

**Note:** These characteristics are based on the assumption that leakage is negligible and appropriate polarity and recombination corrections are applied.

Relative dosimetry of small field often involve the determination of central axis depth dose, tissue phantom ratio, lateral beam profiles and field output factors.

#### 2.1.4 Plastic scintillation detector (PSD)

According to the challenges of small fields dosimetry, selecting a proper detector must have a special consideration. The necessary properties of the desired detector are high spatial resolution, high signal with low noise, physical and electron density equivalence. PSD is the one of the commonly detectors used in small fields due to the advantages of small sensitive volume and water-equivalent density. Moreover, various studies have indicated that perturbation correction factors for plastic scintillators are close to one.<sup>(11)</sup>

The main disadvantage of plastic scintillator system is Cherenkov light generated from optic fiber cable that possible to increase the over signal.<sup>(12)</sup> Using PSD is not straightforward as with other detector systems. It requires a certain irradiation geometry in a solid phantom and the system that removes noise of Cherenkov light.

The scintillation mechanism in organic materials like plastic arises from transitions in the energy levels of organic molecules. When the charged particle passes through, kinetic energy is absorbed by the organic molecules, and electrons are excited to the upper levels of variety of excited states – the singlet states (spin = 0) are labeled  $S_1$ ,  $S_2$ ,  $S_3$  as shown in Figure 2.2.<sup>(13)</sup>

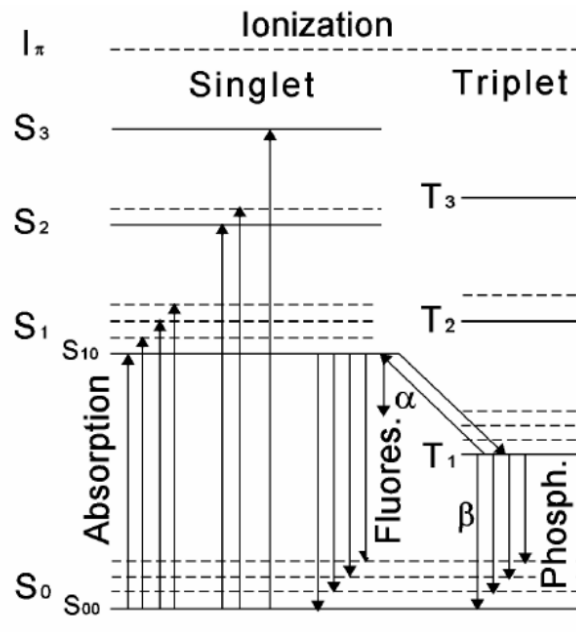


Figure 2.2 Energy levels of organic molecules inside plastic scintillation detector.

For organic scintillators, the spacing between  $S_0$  and  $S_1$  is 3 to 4 eV, the spacing between the upper states is much smaller. Scintillation light, prompt fluorescence, is emitted in transitions between  $S_1$  and the ground state. The  $T_1$ - $S_0$  transitions give rise to phosphorescence (delayed emission). The wavelength of the emitted phosphorescence is longer than the wavelength of the fluorescent light. The phosphorescent light can be discriminated from the scintillation light on the basis of timing and wavelength.

### 2.1.5 Volumetric-modulated arc therapy

In a volumetric-modulated arc therapy (VMAT), the gantry moves continuously with the moment of the multileaf collimator (MLC) and varying of dose rate throughout the arc. For the dose calculation, treatment planning system (TPS) determines the absorbed dose by sampling the delivery at a number of discrete angles. In order to create a satisfactory dose plan with a single arc, it is necessary to

optimize the field shapes and beam intensities from a large number of gantry angles. However, the larger sampled number of gantry angles, the more difficult to optimize within the MLC leaf motion constraints. The biggest advantage of a VMAT delivery system is the reductions in both treatment times and monitor unit (MU) over the conventional intensity modulated radiation therapy (IMRT). Shorter overall delivery times result in decreasing the amount of patient motion that occurs during treatment.<sup>(14)</sup>

### 2.1.6 Stereotactic body radiation therapy

The stereotactic body radiation therapy (SBRT) refers to stereotactic radiotherapy mostly treating the tumors in the spine, lung, liver, pancreas and prostate with a high dose per fraction (6 to 30 Gy), in a hypofractionated regimen of five or fewer fractions. Due to a few fractions with a high dose per fraction, the conformation of a high dose to the target volume together with a rapid fall-off of dose outside the target volume is critical importance in minimizing damage to normal organs.

The main characteristics that distinguish SBRT from conventional 3D and IMRT radiotherapy are allowance of small or no margins for beam penumbra, stringent need for patient immobilization and respiratory motion management, and higher frequency of patient monitoring and geometric verification through image guidance.<sup>(14)</sup>

## 2.2 Reviews of related literatures

Ananda Giri Badu Alagar et al,<sup>(1)</sup> evaluated the accuracy of four model-based algorithms, X-ray Voxel Monte Carlo (XVMC) from Monaco, Superposition (SP) from CMSXio, AcurosXB (AXB) and analytical anisotropic algorithm (AAA) from Eclipse against the measurement. Measurements are performed by using the Exaradin W1

plastic scintillation detector in solid water phantom with heterogeneities (air, lung, bone and aluminum) as shown in Figure 2.3 irradiated with 6 and 15 MV photons of square fields ranging from 1x1 to 4x4 cm<sup>2</sup>. There are two positions of heterogeneous slabs, one setup being the nearer depth of dose maximum ( $D_{max}$ ) called  $D_{near}$  and another farther from  $D_{max}$  called  $D_{far}$ .

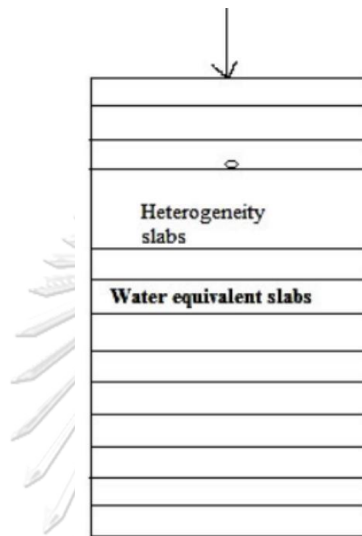


**Figure 2.3** Sample setup showing scintillator plate reserved to measure the dose at entrance junction of heterogenous slab. The detector is shown as a small circle and the arrow shows the beam entry point on the phantom.<sup>(1)</sup>

The percentage normalized root mean squared deviation (%NRMSD) is calculated, which represents the depth dose deviation against measurement. The formula of %NRMSD is

$$\%NRMSD = \frac{RMSD}{(Measured_{max} - Measured_{min})} \times 100$$

Where RMSD is root mean square deviation is calculated as

$$RMSD = \sqrt{\frac{1}{n} \sum_{i=1}^n (Measured_i - Calculated_i)^2}$$

Where n is the number of depth points for which depth dose is calculated.



The results showed that in the case of air and lung heterogeneity, for both 6 and 15 MV, all algorithms showed maximum deviation at field size of  $1 \times 1 \text{ cm}^2$  and gradually reduced when field size increased, except AAA. In the case of aluminum and bone, each deviation of all algorithms is small especially in high energy of 15 MV. In all heterogeneity, the deviation between the measured and calculated dose of  $D_{\text{near}}$  setup was higher than  $D_{\text{far}}$  setup. All algorithms showed maximum deviation in low-density materials compared to high-density materials. The examples of their results are shown in Figure 2.4 and 2.5.

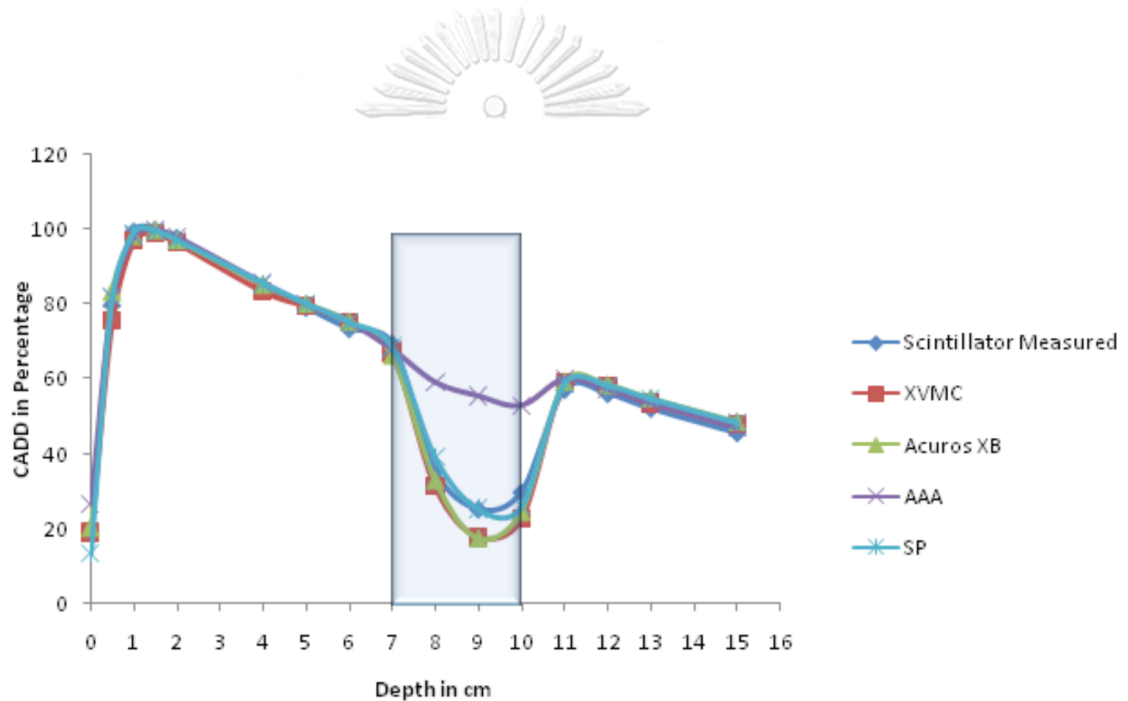


**Figure 2.4** The central axis depth dose (CADD) curves of measured and four algorithms for lung heterogeneity in 6 MV far to  $D_{\text{max}}$  setup for field size  $1 \times 1 \text{ cm}^2$ .

Lung heterogeneity region is shown in shaded area.

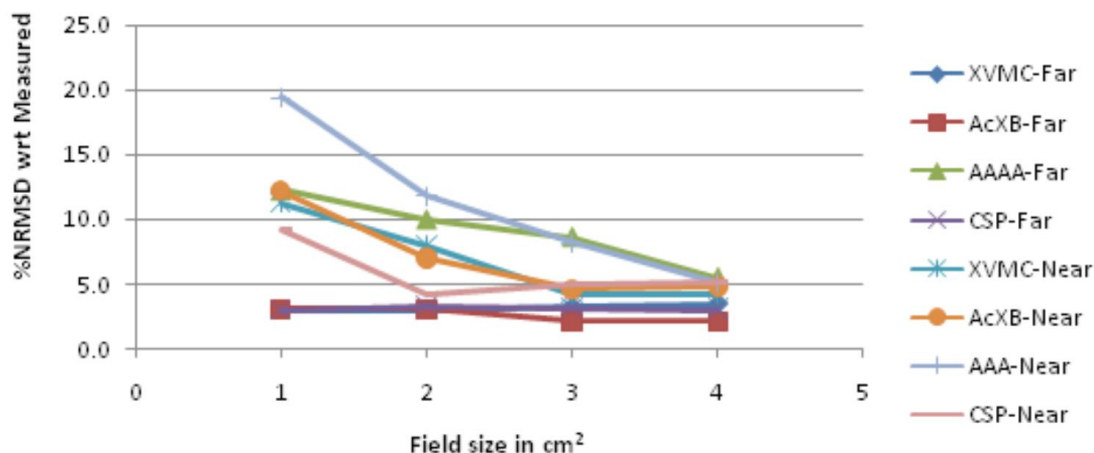


**Figure 2.5** Curves of %NRMSD respect to W2 plastic scintillator measurement for every field size in two different lung heterogeneity setups for 6 MV photon beam.

Jinyu Xue et al,<sup>(15)</sup> evaluated a plastic scintillator for the small field dosimetry measurement and verified the accuracy of the measured dose in comparison with Monte Carlo calculation in a heterogeneous medium. Their study was performed with CyberKnife planning and delivery system. The measurement setup consisted of a custom-made solid lung phantom with the insertion of Exradin W1 plastic scintillator and Exradin A16 ionization chamber and was done for a series of cone sizes ranging from 5 to 60 mm. The doses were calculated by Monte Carlo algorithm in Multiplan workstation and the differences between the calculated and measured dose was less than 3% for all cone sizes, ranging from 5 to 60 mm. The measured dose from the plastic scintillator calibrated to the ionization chamber reading was also within 3% of the Monte Carlo calculation in the lung phantom for cone sizes larger than 20 mm.

Antonella Fogliata et al,<sup>(20)</sup> evaluated and determined relative figures of merit of new algorithm for photon dose calculation in heterogeneous media. Their study was carried out in virtual phantoms that was characterized by simple geometrical structures. The heterogeneous medium was included in a phantom built of skeletal-muscle (phantom A): normal lung ( $0.198 \text{ g/cm}^3$ ), light lung ( $0.035 \text{ g/cm}^3$ ) and bone

( $1.789 \text{ g/cm}^3$ ). Another phantom (phantom B) was built of adipose material including thin layers of bone ( $1.798 \text{ g/cm}^3$ ), adipose ( $0.920 \text{ g/cm}^3$ ), cartilage ( $1.475 \text{ g/cm}^3$ ) and air ( $0.0012 \text{ g/cm}^3$ ) as shown in Figure 2.6.

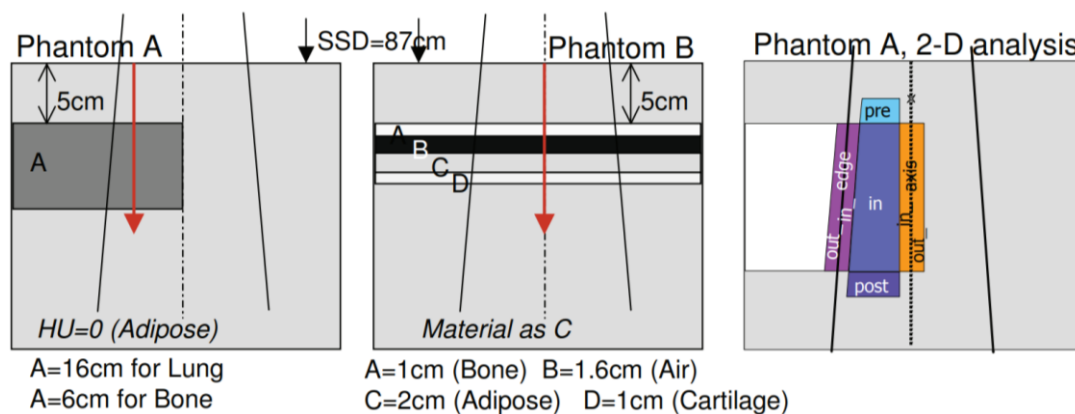


**Figure 2.6** Geometrical layout of phantoms. Setting A on the left; and setting B in the middle; sectors used in the 2D gamma analysis for setting A on the right.

The calculations were performed for 6 and 15 MV with large field size of  $13 \times 13 \text{ cm}^2$  and small field size of  $2.8 \times 13 \text{ cm}^2$ . Monte Carlo calculations were assumed as references. Acuros XB gave an average gamma agreement, with a 3 mm/3% criteria, of 100%, 86% and 100% for normal lung, light lung and bone settings, respectively. The study showed that Acuros XB provides an accurate alternative to Monte Carlo calculations for dosimetry in heterogeneous media.

## CHAPTER III

### RESEARCH METHODOLOGY

#### 3.1 Research design

This research was observational design in the type of analytical study.

#### 3.2 Research design model

This study was separated into three major parts. The first part was a study of W2 plastic scintillator characteristics in water. The second part was a comparison of percentage depth dose (PDD) inside solid water phantom where heterogeneity slabs were introduced at 3 cm depth. The final part was a clinical application that compare measured dose to calculated dose inside CIRS thorax phantom. The study diagram of each part is shown in Figure 3.1 – 3.3.

##### 3.2.1 W2 plastic scintillator characteristics in water

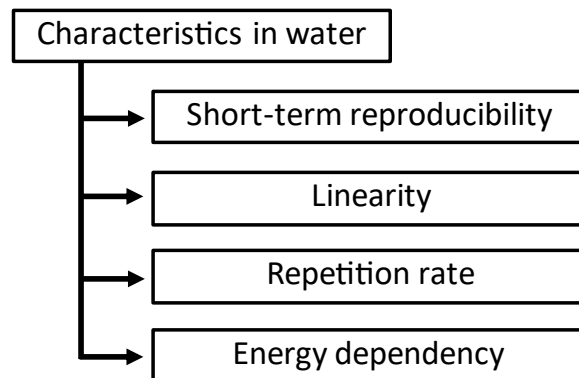


**Figure 3.1** Research design model of W2 plastic scintillator characteristics in water

### 3.2.2 Percentage depth dose in heterogenous media

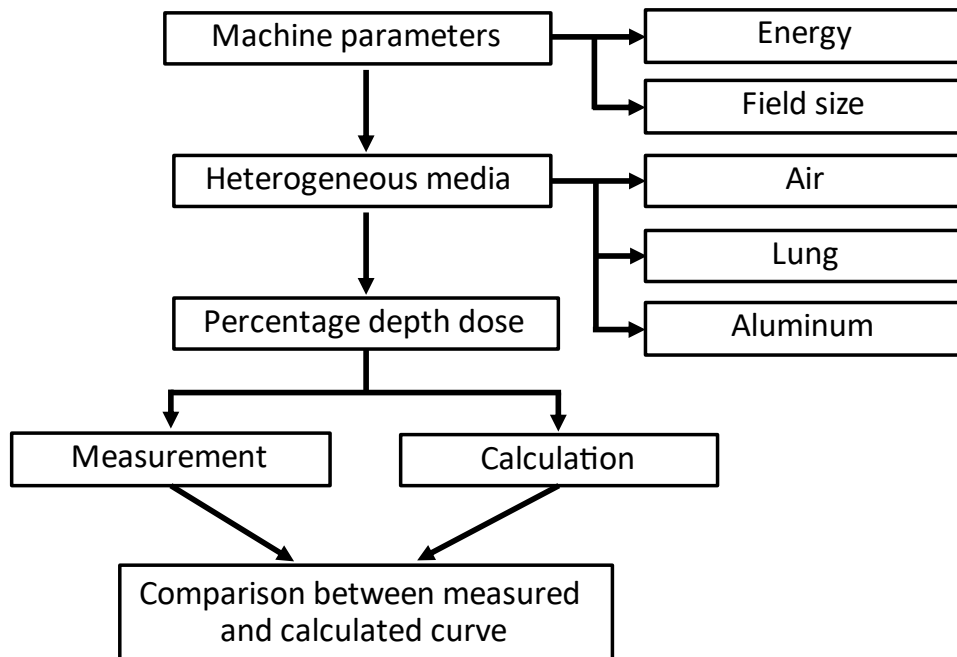


Figure 3.2 Research design model of percentage depth dose in heterogenous media

### 3.2.3 Clinical application in CIRS thorax phantom

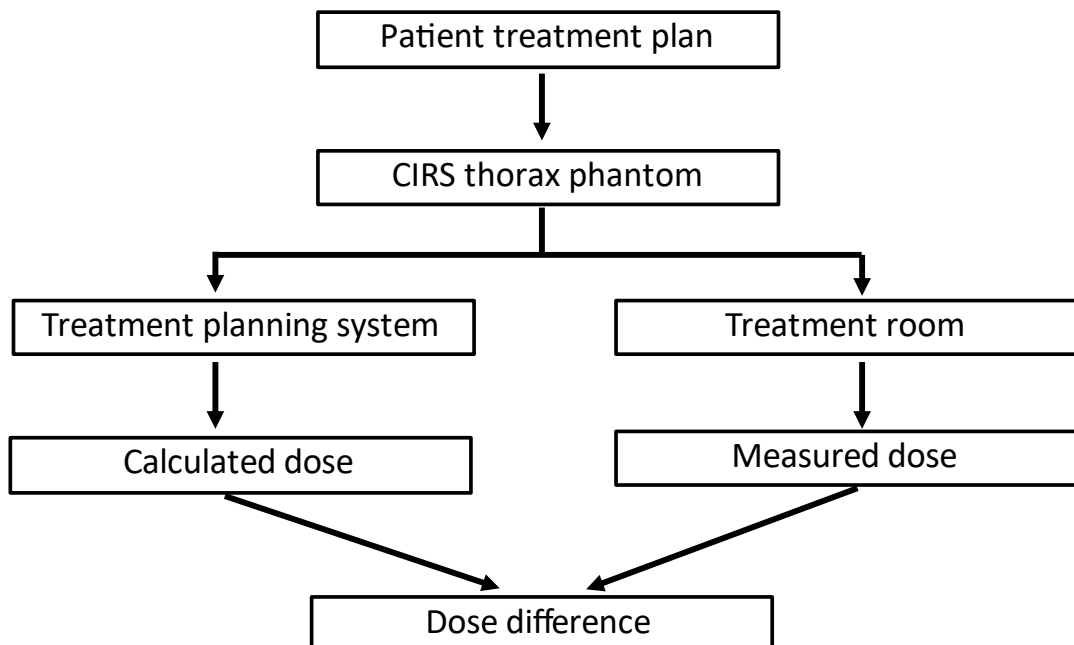


Figure 3.3 Research design model of clinical application in CIRS thorax phantom

### 3.3 Conceptual framework

The difference between measured and calculated dose is affected by several factors as shown in Figure 3.4.

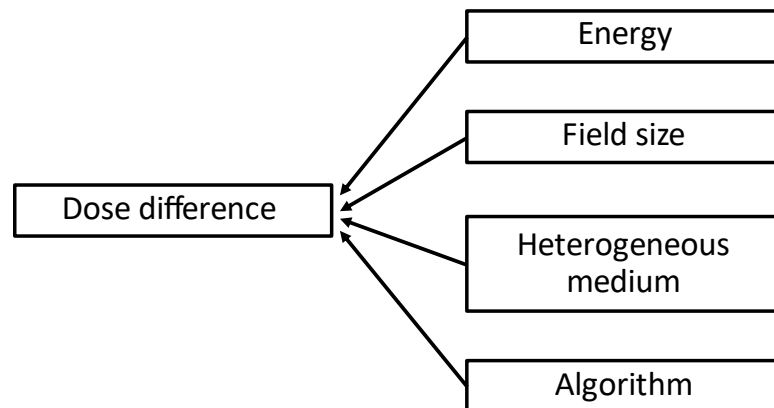


Figure 3.4 Conceptual framework

### 3.4 Research questions

- 3.4.1 What are the W2 plastic scintillator characteristics in water?
- 3.4.2 What are the differences between measured dose from W2 plastic scintillator and calculated dose from algorithm calculation?

### 3.5 Materials

The materials used in this study were supplied from the Division of Radiation Oncology, King Chulalongkorn Memorial Hospital.

#### 3.5.1 Varian TrueBeam™ linear accelerator

Linear accelerator or linac is radiotherapeutic machine that can deliver high-energy photon to the tumor cell. This study employed Varian TrueBeam™ linac machine (Varian Medical System, Palo Alto, CA, USA), as shown in Figure 3.5. TrueBeam is the modern medical linac commercially available with millennium-120 leaf multi-leaf collimator. It can deliver flattening filter free (FFF) and with flattening

filter (WFF) photon beams. It is equipped with four photon beam energies (6 FFF, 6 MV, 10 FFF and 10 MV). The maximum dose rate for the 6 WFF and 10 WFF is 600 MU/min, whereas 6 FFF and 10 FFF has a maximum dose rate of 1400 MU/min and 2400 MU/min respectively.<sup>(16)</sup>



Figure 3.5 Varian TrueBeam™ linear accelerator

### 3.5.2 CT simulator

The SOMATOM Definition AS 64-slice CT simulator as presented in Figure 3.6, (Siemens Healthcare GmbH, Erlangen, Germany) was used in this study to simulate structure and collect electron density data from solid phantom for dose calculation in treatment planning system. Aperture bore diameter of Siemens SOMATOM CT simulator is 800 mm. The distance from tube to isocenter and tube to detector is 595 mm and 1085 mm, respectively. The tube voltage settings are 80, 120, 140 kVp and 80/140 kVp combinations for dual energy CT option. The tube current setting is in the range of 20 – 666 mA.



**Figure 3.6** Siemens SOMATOM CT simulator

### 3.5.3 Exradin W2 plastic scintillator

The Exradin W2-1x1 (Standard Imaging, Middleton, WI) as shown in Figure 3.7 features a scintillating fiber with 1.0 mm diameter and 1.0 mm long ( $0.0008 \text{ cm}^3$  volume), improving measurement resolution for the smallest field characterization measurements. It has a physical density of  $1.05 \text{ g/cm}^3$  and is made of polystyrene with ABS plastic enclosure and polyimide stem.

The plastic scintillator operates when the passage of ionizing radiation travels through a scintillating material and excites the electron of the atoms in the material to excited state. When the electron decay to the ground state, it emits photons which are collected by a photodetector and light signals are measured by a high-precision electrometer called MAXSD.

However, the plastic scintillator has a problem with Cerenkov emissions in the optical fiber. The Cerenkov emissions are created when the optical fiber connecting scintillating material to the photodiode is irradiated. The amount of light produced is proportional to the irradiated length of the optical fiber, and measurement results must be corrected to account for this phenomenon.



The W2 system features Cerenkov corrected measurement signals that can be converted to a proportional analog output, which can be read by the electrometer. This allows the Exradin W2 system to be connected to a water phantom system for scanning.<sup>(17)</sup>

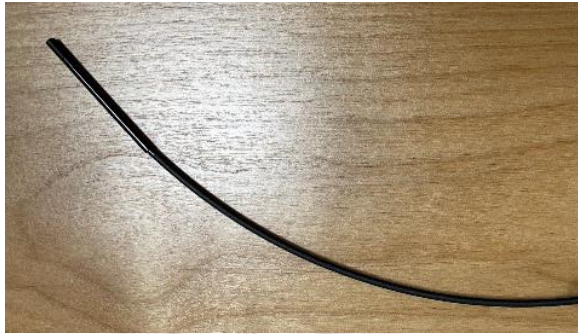


**Figure 3.7** Exradin W2 plastic scintillation detector (W2-PSD)

#### **3.5.4 Solid water slab phantom**

The solid water slab phantom (Gammex rmi, Middleton WI) is used to replace the water phantom. It is made in 30x30 cm<sup>2</sup> square slabs in various thicknesses with a density of 1.02 g/cm<sup>3</sup> and the atomic number of 5.95 as shown in Figure 3.8.<sup>(18)</sup>



**Figure 3.8** Solid water slab phantom

#### **3.5.5 Heterogeneous slab phantom**

There are 3 types of heterogeneous slab phantom were used in this study which are air (Styrofoam), lung (cork) and aluminum whose physical densities are 0.001, 0.27 and 2.7 g/cm<sup>3</sup>, respectively. Each heterogeneous slab was designed in a

30x30 cm<sup>2</sup> square slab with the desired hole for Exradin W2 plastic scintillator insertion as shown in Figure 3.9.

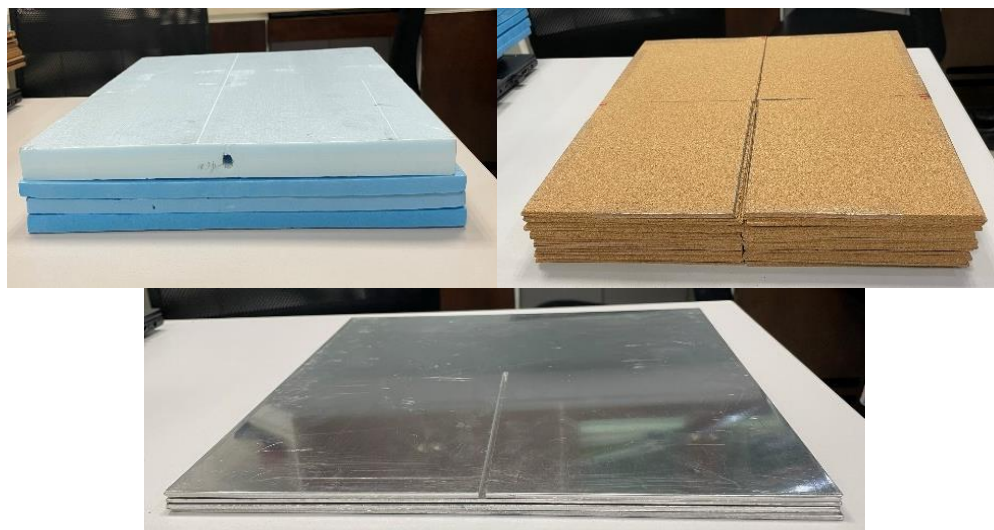


**Figure 3.9** Heterogeneous slab phantom, air (top-left), lung (top-right) and aluminum (bottom)

### 3.5.6 CIRS thorax phantom

The CIRS thorax phantom, as shown in Figure 3.10, is a precision instrument for investigating and minimizing the impact of tumor motion inside the patient's lung. It provides known, accurate, and repeatable three-dimensional target motion inside a tissue-equivalent phantom. It is designed for comprehensive analysis of image acquisition, planning, and dose delivery in image-guided radiation therapy. The CIRS thorax phantom represents an average human thorax in shape, proportion, and composition. A lung equivalent rod containing a spherical target which designed for various detectors insertion into the lung equivalent lobe of the phantom.<sup>(19)</sup>



Figure 3.10 CIRS thorax phantom

### 3.5.7 Eclipse™ treatment planning system

Eclipse™ treatment planning system software version 16.1 (Varian Medical System, Inc., Palo Alto, CA, USA) is a planning system that supports external beam radiotherapy including various of photon radiation treatment techniques such as 3D, IMRT and VMAT. There are two photon dose calculation algorithms: Acuros XB algorithm and Analytical Anisotropic Algorithm (AAA).

The Acuros XB algorithm uses the deterministic radiation transport solutions of the linear Boltzmann transport equation (LBTE) to eliminate the statistical noise in the calculated dose. It directly accounts for the effect of heterogeneities by taking their chemical compositions apart from density.<sup>(20)</sup>

The analytical anisotropic algorithm (AAA) dose calculation based on the superposition-convolution method and operated by Eclipse TPS.<sup>(21)</sup> The AAA is not accounting for chemical properties of tissue, so the calculated dose can be defined as dose rescaled to water according to the specific density.

## 3.6 Methods

This study can be separated to three major parts. The first part was the study of W2 plastic scintillator characteristics in water. The second part was the percentage

depth dose curves in heterogenous media comparison between the curve retrieved from W2 plastic scintillator and from algorithm calculation. The final part was a clinical application in CIRS thorax phantom where the difference between measured and calculated dose was determined.

### 3.6.1 Pre-irradiation: plastic scintillator calibration

W2 system is a web-based interface that allows user controls the electrometer and collects measured data on the personal computer. The electrometer in W2 system is called MAXSD. However, the main problem of the plastic scintillator process is the Cerenkov emission which is an unwanted signal coming from the optical fiber part when it is irradiated. Hence, the plastic scintillator system has to design the electrometer that can eliminate this Cerenkov light from the real signal. The Cerenkov light elimination of the MAXSD is included in calibration process of the plastic scintillator system. This study used small field water tank method that can be followed by the manufacturer's manual to calibrate the system.

#### 3.6.1.1 Small field water tank calibration method

1. The plastic scintillator was positioned inside the Cerenkov light ratio (CLR) calibration bracket and the optical fiber was placed in the curved channel for the maximum fiber configuration. The center of the active area of the fiber was centered within the radiation field as shown in Figure 3.11.

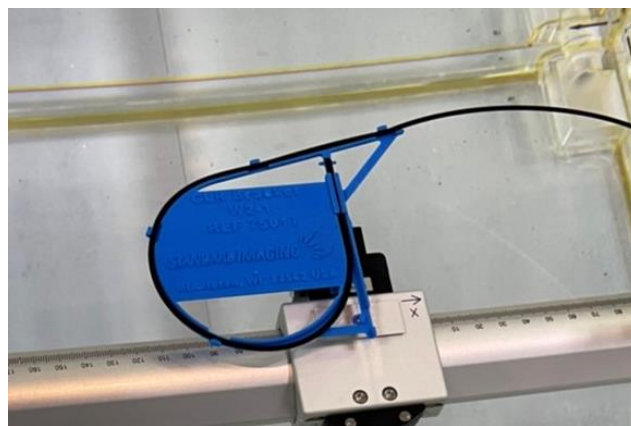


Figure 3.11 Maximum configuration setup

2. The water tank was set at 100 cm SSD and the plastic scintillator with the bracket was placed at 1.5 cm depth.
3. The machine parameters were adjusted by the following conditions:
  - 6 FFF photon energy
  - 6 x 6 cm<sup>2</sup> field size
  - 200 MU
  - 800 MU/min repetition rate
4. The measurement was repeated several times to generate a stable average value.
5. The optical fiber was repositioned in the straight channel for the minimum fiber configuration as shown in Figure 3.12.

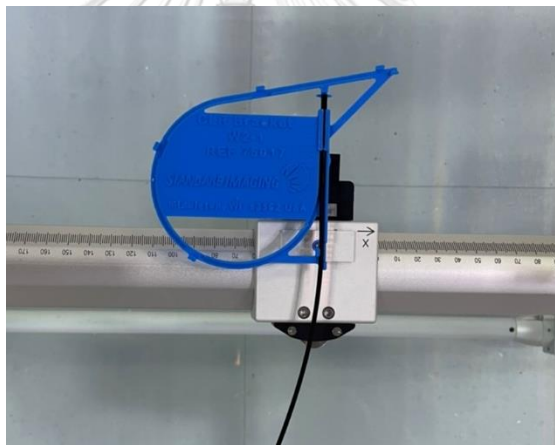


Figure 3.12 Minimum configuration setup

6. The same machine parameters were delivered to the maximum fiber configuration setup.
7. The measurement was repeated several times to generate a stable average value.
8. The measured signal was separated into blue and green channel by the MAXSD and showed real-time value on personal laptop screen as shown

in Figure 3.13. The MAXSD calculated the Cerenkov light ratio (CLR) and gain value automatically by these following formulas.

$$\text{CLR} = \frac{(\text{Blue}_{\text{MAX}} - \text{Blue}_{\text{MIN}})}{(\text{Green}_{\text{MAX}} - \text{Green}_{\text{MIN}})}$$

$$\text{Gain} = \frac{D_{\text{ref}}}{[\text{Blue}_{\text{ref}} - (\text{Green}_{\text{ref}} \times \text{CLR})]}$$

Where **CLR** is Cerenkov light ratio.

**Gain** is dose conversion value.

**Blue<sub>MAX</sub>** is blue channel signal, maximum fiber configuration.

**Green<sub>MAX</sub>** is green channel signal, maximum fiber configuration.

**Blue<sub>MIN</sub>** is blue channel signal, minimum fiber configuration.

**Green<sub>MIN</sub>** is green channel signal, minimum fiber configuration.

**Blue<sub>ref</sub>** is blue channel signal, maximum fiber configuration.

**Green<sub>ref</sub>** is blue channel signal, maximum fiber configuration, reference dose measurement.

**D<sub>ref</sub>** is dose delivered to the scintillator in the reference field irradiation.

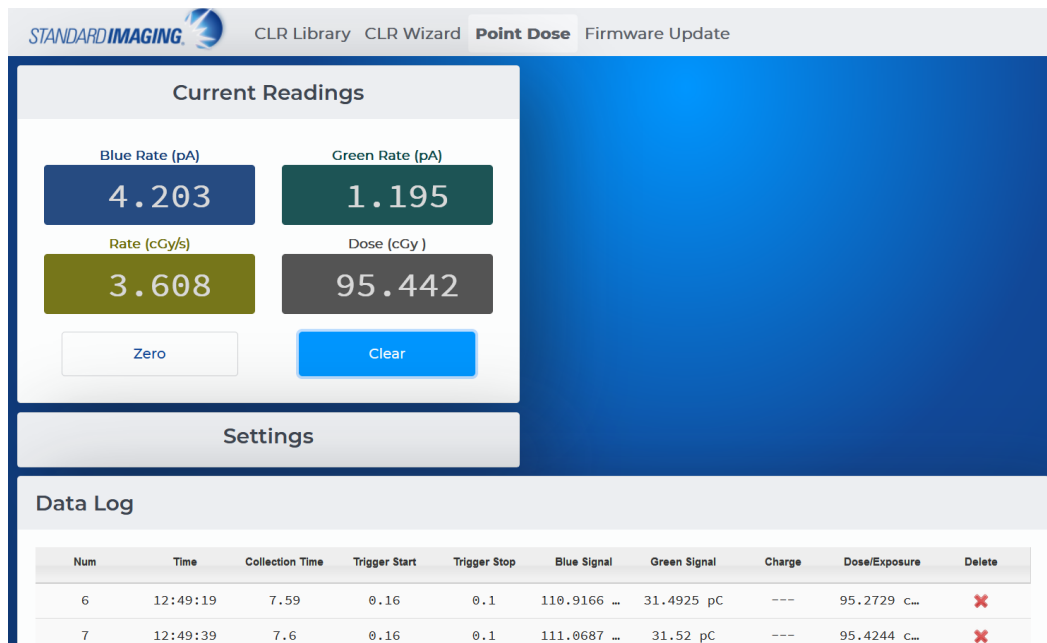


**Figure 3.13** The example of W2 plastic scintillator system web-based interface for the point dose measurement

9. For the reference condition, this study used  $10 \times 10 \text{ cm}^2$  field size, 6 FFF photon energy, 100 MU and position of the plastic scintillator was placed at 1.5 depth. From these machine parameters and setup, it results to  $D_{\text{ref}}$  equals to 100 cGy.
10. Each step of W2 plastic scintillator calibration procedures can be followed by the web-based manufacturer's direction as shown in Figure 3.14.



STANDARDIMAGING. CLR Library CLR Wizard Point Dose Firmware Update

**Step 1 - Obtain Max Fiber Values (Complete)**

**Max Fiber Checklist**

- Field size set
- Place fiber in maximum configuration
- Set depth
- Use trigger level for collection start (optional)

Start Trigger Level (pA)

Stop Trigger Level (pA)

**Start**

**Max Fiber Data Log**

Num	Collection Time	Trig Start (pA)	Trig Stop (pA)	Blue Charge (pC)	Green Charge (nC)	Delete
2	7.6	0.16	0.1	149.324295	66.003204	✘
3	7.6	0.16	0.1	149.215225	65.971375	✘
4	7.6	0.16	0.1	149.270996	65.996605	✘
5	7.6	0.16	0.1	149.246002	66.054703	✘

Blue Avg: 149.3500 pC   Blue Std Dev: 0.1755   Green Avg: 66.0579 pC   Green Std Dev: 0.1863

**Step 2 - Obtain Min Fiber Values (Incomplete)**

**Step 3 - Dose Calibration (Optional)**

**Step 4 - View and Save CLR Values**

---

**Step 1 - Obtain Max Fiber Values (Complete)**

**Step 2 - Obtain Min Fiber Values (Complete)**

**Step 3 - Dose Calibration (Complete)**

**Dose Calibration**

- Enable Dose Calibration

Dose Reference  cGy

**Dose Checklist**

- Reference field size set
- Set depth reference
- Use trigger level for collection start (optional)

Start Trigger Level (pA)

Stop Trigger Level (pA)

**Start**

**Dose Fiber Data Log**

Num	Collection Time	Trig Start (pA)	Trig Stop (pA)	Blue Charge (pC)	Green Charge (nC)	Delete
2	7.6	0.16	0.1	119.116066	37.499779	✘
3	7.6	0.16	0.1	119.126579	37.478439	✘
4	7.6	0.16	0.1	119.1716	37.488644	✘
5	7.59	0.16	0.1	119.111473	37.483887	✘

Blue Avg: 119.1316 pC   Blue Std Dev: 0.0213   Green Avg: 37.4860 pC   Green Std Dev: 0.0076

**Step 4 - View and Save CLR Values**

**Figure 3.14** The example of W2 plastic scintillator system web-based interface in the calibration process

### 3.6.2 The W2 plastic scintillator characteristics in water

The characteristics in water of W2 plastic scintillator consist of short-term reproducibility, linearity, repetition rate response and energy dependency.



### 3.6.2.1 Short-term reproducibility

The procedures of the short-term reproducibility study were as follows:

1. The water tank was set at 100 cm SSD and the plastic scintillator was placed at 1.5 cm depth.
2. The machine parameters were adjusted by the following conditions:
  - 6 FFF photon energy
  - 4 x 4 cm<sup>2</sup> field size
  - 100 MU
  - 400 MU/min repetition rate
3. The measurements were performed 10 times to observe the short-term reproducibility of the plastic scintillator.

### 3.6.2.2 Linearity

The procedures of the linearity study were as follows:

1. The water tank was set at 100 cm SSD and the plastic scintillator was placed at 1.5 cm depth.
2. The machine parameters were adjusted by the following conditions:
  - 6 FFF photon energy
  - 4 x 4 cm<sup>2</sup> field size
  - 400 MU/min repetition rate
3. The measurement was performed with varying monitor units from 10 to 2000 MU.

### 3.6.2.3 Repetition rate response

The procedures of the repetition rate study were as follows:

1. The water tank was set at 100 cm SSD and the plastic scintillator was placed at 1.5 cm depth.

2. The machine parameters were adjusted by the following conditions:
  - 6 FFF photon energy
  - 4 x 4 cm<sup>2</sup> field size
  - 100 MU
3. The measurement was performed with varying repetition rates from 10 to 2000 MU.

#### 3.6.2.4 Energy dependency

The procedures of the dependency study were as follows:

1. The water tank was set at 100 cm SSD and the plastic scintillator was placed at  $D_{\max}$  position (1.5 cm depth for 6 FFF and 2.5 cm depth for 10 FFF).
2. The machine parameters were adjusted by the following conditions:
  - 6 FFF and 10 FFF photon energy
  - 10 x 10 cm<sup>2</sup> field size
  - 200 MU
  - 800 MU/min repetition rate
3. The measurement was performed with the varying of two energy levels of 6 and 10 FFF.

#### 3.6.3 Percentage depth dose in heterogenous media

The procedures of percentage depth dose study were as follows:

1. The 30 cm-height solid phantom composed of solid water slabs and heterogeneity slabs of air, lung and aluminum were inserted at 3 cm depth as shown in Figures 3.15 and 3.16.

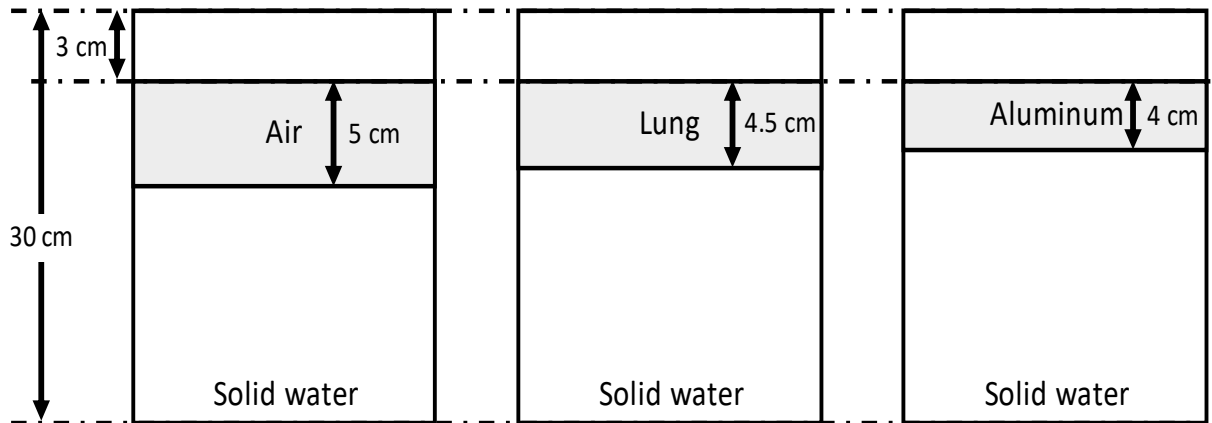
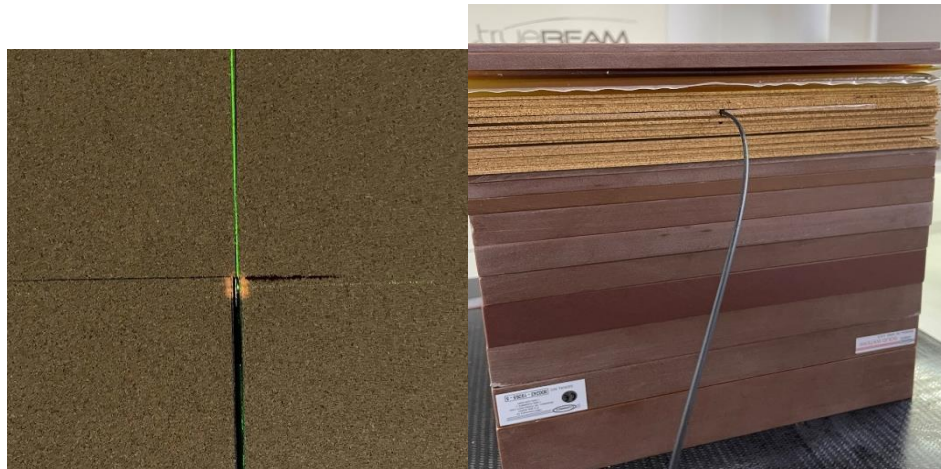


Figure 3.15 Heterogeneous phantom diagram

2. The machine parameters were adjusted by the following conditions:
  - 100 cm SSD
  - 200 MU
  - Energy: 6 and 10 FFF
  - Field size: 1x1, 2x2, 3x3 and 4x4 cm<sup>2</sup>
  - Repetition rate: 1400 MU/min (for 6 FFF) and 2400 MU/min (for 10 FFF)
3. The position of the plastic scintillator was moved along the central beam axis inside the solid phantom.
4. The measurement was performed with varying of energy, field size and heterogenous media. At each step, the measurement was performed 3 times to find the average and the resolution of percentage depth dose curve of each heterogeneous media depending on the thickness of the heterogeneity slab.



**Figure 3.16** Heterogeneous phantom measurement setup

5. The comparison of percentage depth dose curve from the measurement (plastic scintillator and film) and calculation (Acuros and AAA) was reported in form of graph and table of %NRMSD.

#### 3.6.4 Clinical application in CIRS thorax phantom

The procedures of clinical application in CIRS thorax phantom were as follows:

1. The CIRS thorax phantom with insertion of a plastic scintillator was scanned by CT simulator as shown in Figure 3.17 and CT data was transferred to TPS.



Figure 3.17 CIRS thorax phantom scanning

2. The 10 treatment plans of lung cancer patient who were treated by SBRT-VMAT techniques were randomly selected. The plans were transferred and recalculated to CIRS phantom images in Eclipse treatment planning system. The absolute dose inside the sensitive volume of the plastic scintillator was calculated as shown in Figure 3.18.

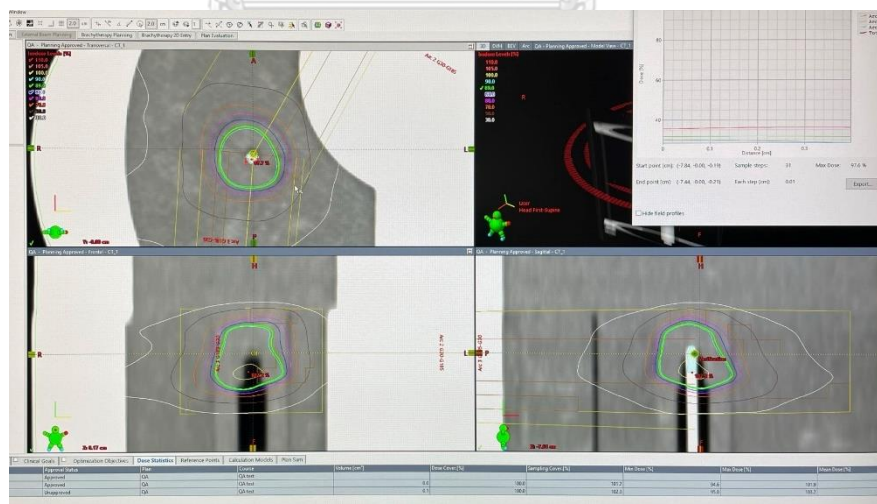


Figure 3.18 Calculated dose inside CIRS thorax phantom

3. Treatment plans were exported to the treatment room. The plastic scintillator was used to measure the dose inside the CIRS thorax phantom as shown in Figure 3.19.

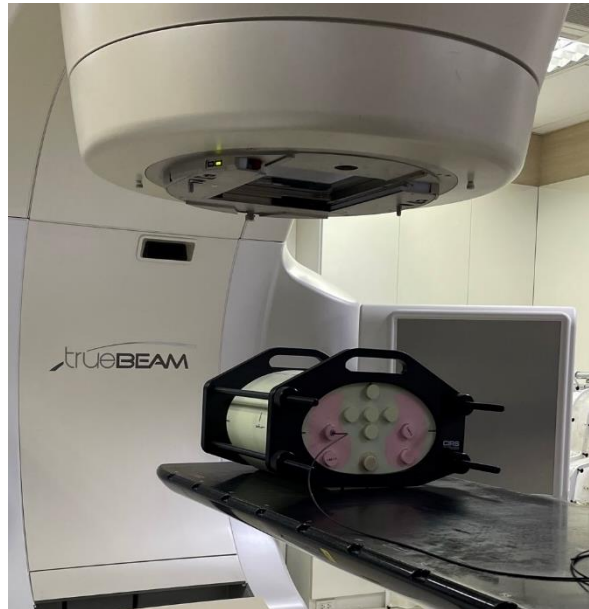


Figure 3.19 CIRS thorax phantom measurement setup

4. The difference between measured and calculated dose was reported.

### 3.7 Statistical analysis

1. Average and standard deviation were used to present the results.
2. The percentage difference between the measured and calculated dose was defined as

$$\%difference = \frac{(D_{plastic} - D_{cal}) \times 100}{D_{cal}}$$

Where  $D_{plastic}$  is measured dose from a plastic scintillator

$D_{cal}$  is calculated dose from TPS

3. The percentage normalized root mean squared deviation (%NRMSD) was defined as

$$\%NRMSD = \frac{RMSD}{(Measured_{\max} - Measured_{\min})} \times 100$$

Where RMSD is root mean square deviation is calculated as

$$RMSD = \sqrt{\frac{1}{n} \sum_{i=1}^n (Measured_i - Calculated_i)^2}$$

Where n is the number of depth points for which depth dose is calculated.

### 3.8 Sample size determination

The sample size was determined such that the average difference between measurements and TPS was -0.19% and 0.96% SD for W1 plastic scintillator and VMAT SRS planning with at least 8 Gy fraction dose.<sup>(22)</sup> The sample size can be calculated by using the following equation:

$$n = \frac{2\sigma^2 (z_{\alpha/2} + z_{\beta})^2}{d^2} \approx 8 \text{ cases (at least)}$$

Where  $z$  is the reliability coefficient of the normal distribution with a 95% confidence limit.

For  $\alpha = 0.05$ ,  $z_{\alpha/2} = 1.96$

For  $\beta = 0.10$ ,  $z_{\beta} = 1.2816$

$\sigma^2$  is the variance of difference  $\approx 0.92$

$d$  is the difference of mean = 1.52 Gy

### 3.9 Outcome measurement

This study determined the difference between the measured dose from W2 plastic scintillator and calculated dose from TPS.

### 3.10 Benefit of research

The benefit of this research is to evaluate the accuracy of dosimeters that can be able to use in small field dosimetry.

### 3.11 Ethical consideration

The treatment plans of lung cancer patient were collected and recalculated in phantom on treatment planning system. The research proposal was submitted and approved by Ethic Committee of the Faculty of Medicine, Chulalongkorn University, and Bangkok, Thailand (IRB NO.0511/65). The certificate is shown in APPENDIX.





## CHAPTER IV

### RESULTS

The results were separated to three major parts: W2 plastic scintillator characteristics in water, percentage depth dose in heterogeneous media and clinical application in CIRS thorax phantom.

#### 4.1 W2 plastic scintillator characteristics in water

##### 4.1.1 Short-term reproducibility

The measurements were performed 10 times as shown in Table 4.1. The normalized result of short-term reproducibility was  $1.00 \pm 0.00\%$ .

**Table 4.1** The result of W2 plastic scintillator short-term reproducibility

No.	Dose (cGy)
1	95.39
2	95.42
3	95.43
4	95.47
5	95.43
6	95.27
7	95.42
8	95.50
9	95.35
10	95.44
Average	95.41

$$SD = 0.06$$

$$\% CV = 0.06$$

#### 4.1.2 Linearity

The result showed the linearity with  $R^2 = 1$  of plastic scintillator in range of 10 to 1900 cGy as shown in Figure 4.1.

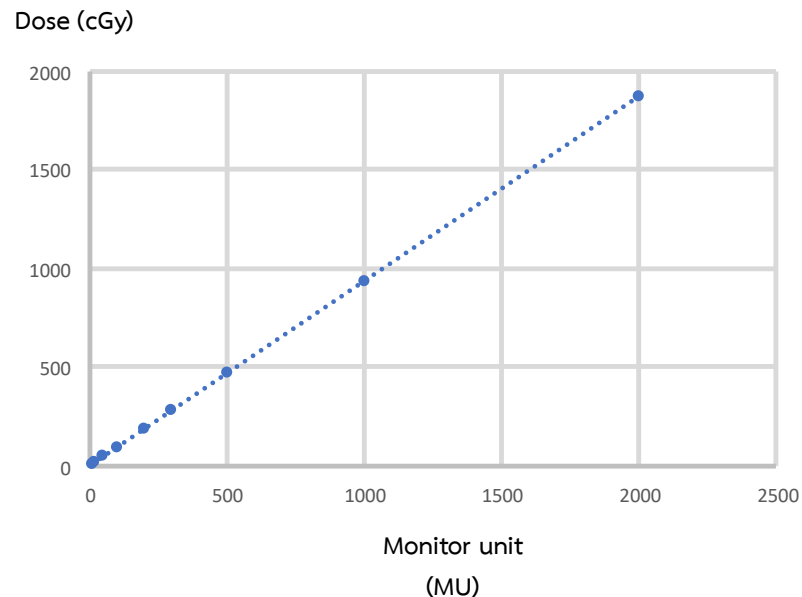


Figure 4.1 Plotted curve of measured dose and monitor unit

#### 4.1.3 Repetition rate response

When the 400 MU/min repetition rate was normalized, the result showed the maximum deviation of repetition rate response about 0.15% in the range of 400 to 1400 MU/min.

##### Normalized repetition rate response

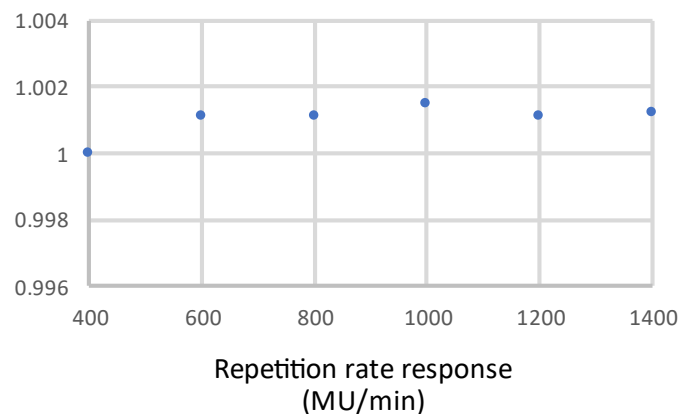


Figure 4.2 The graph of repetition rate response

#### 4.1.4 Energy dependency

The result showed the percentage difference of 0.43% between 6 FFF and 10 FFF as shown in Table 4.2.

**Table 4.2** The result of W2 plastic scintillator energy dependency

No.	Dose (cGy)	
	6 FFF	10 FFF
1	200.00	201.17
2	200.48	201.17
3	200.38	201.24
4	200.39	201.35
5	200.20	201.15
6	200.48	201.34
7	200.44	201.13
8	200.33	201.00
9	200.28	201.13
10	200.28	201.17
Average = 200.33		Average = 201.19
%difference = 0.43%		

#### 4.2 Percentage depth dose in heterogenous media

The graphical results of percentage depth dose curve measured by plastic scintillator and calculated by Acuros and AAA algorithms with different field sizes and energies are shown in Figure 4.3 to Figure 4.8.

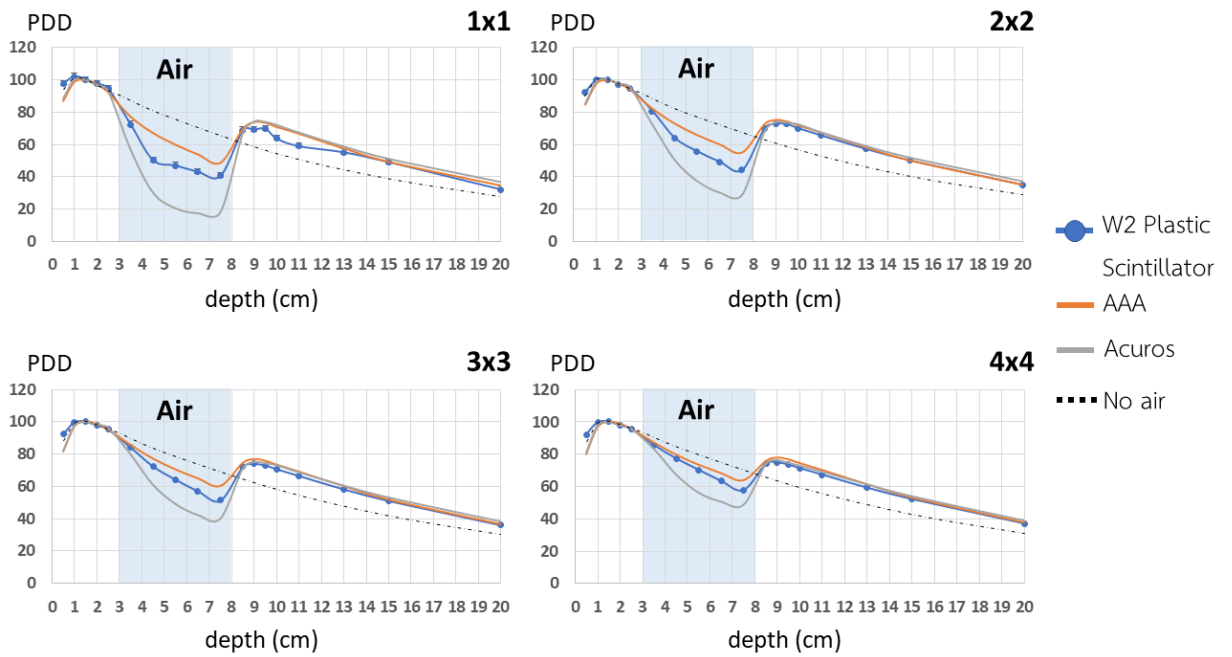


Figure 4.3 The percentage depth dose curve of 6 FFF with different field sizes in air heterogeneous media

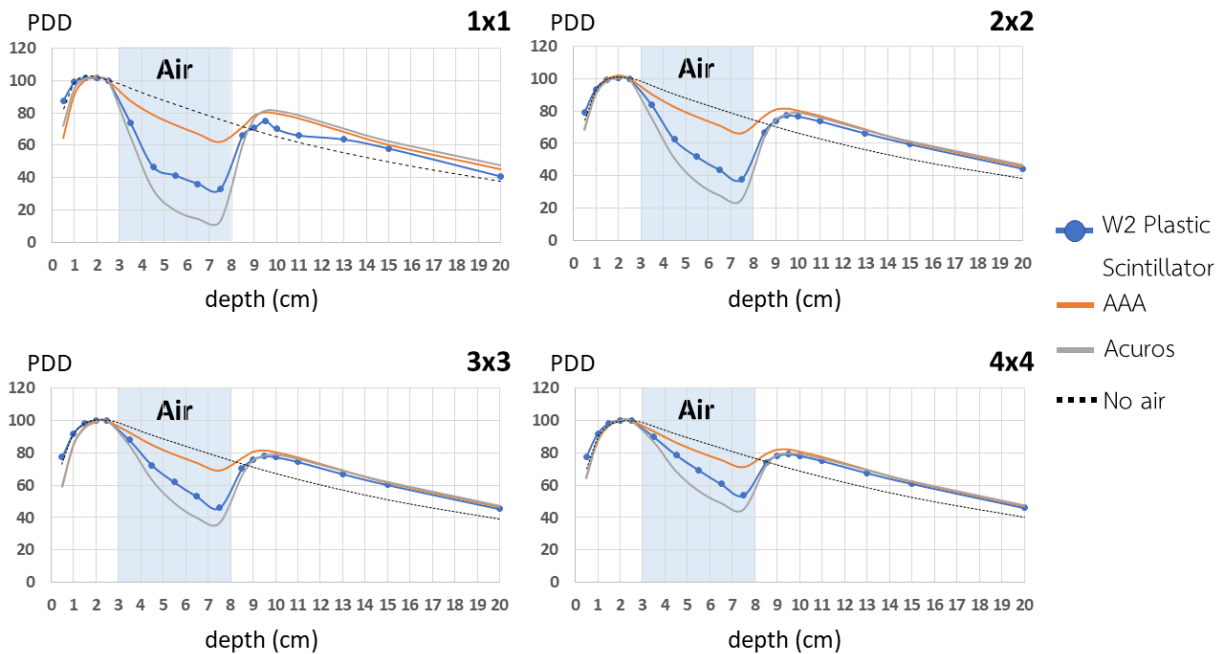


Figure 4.4 The percentage depth dose curve of 10 FFF with different field sizes in air heterogeneous media

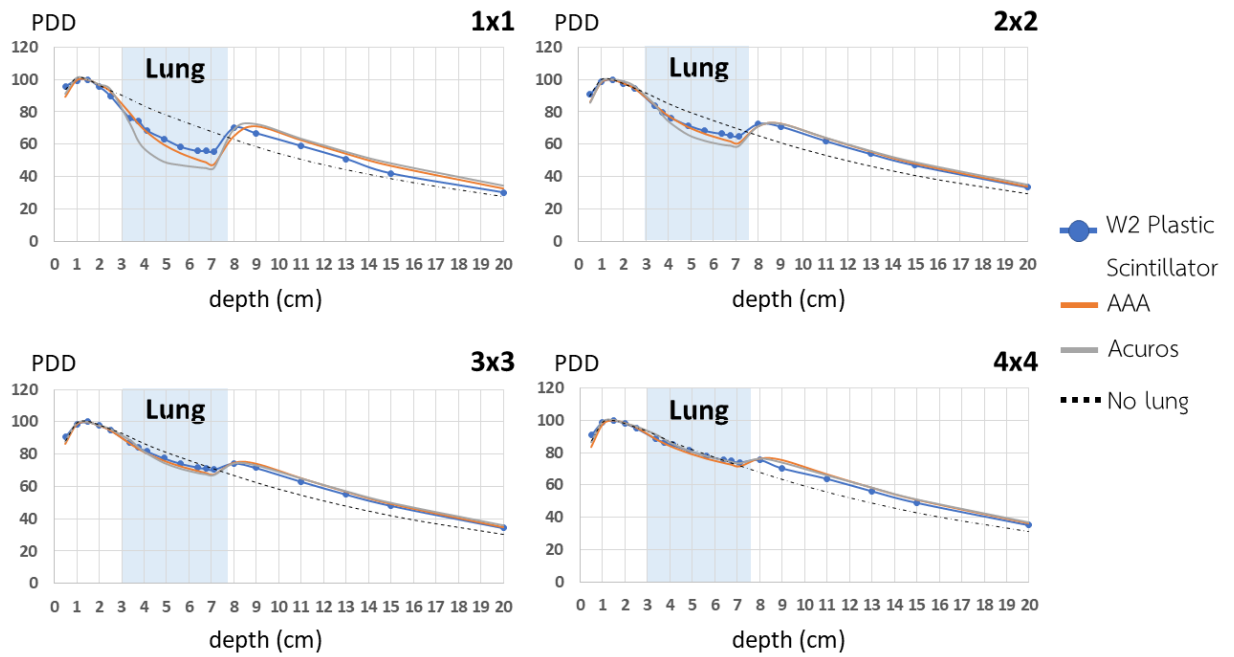


Figure 4.5 The percentage depth dose curve of 6 FFF with different field sizes in lung heterogeneous media

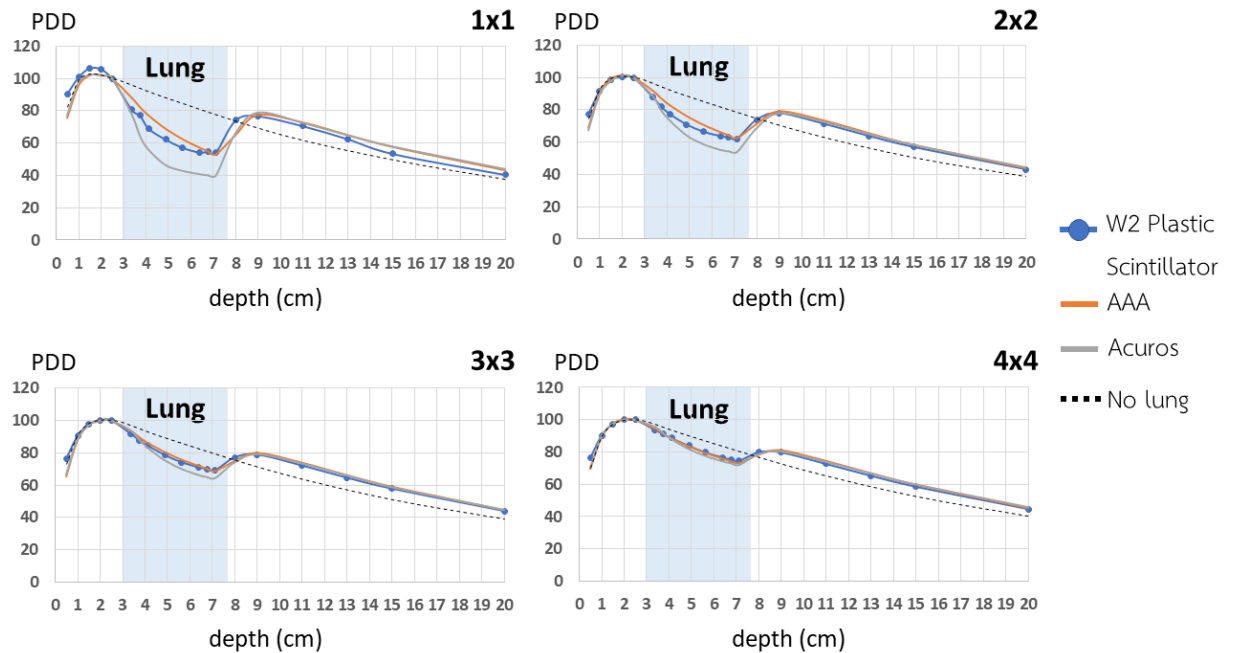


Figure 4.6 The percentage depth dose curve of 10 FFF with different field sizes in lung heterogeneous media

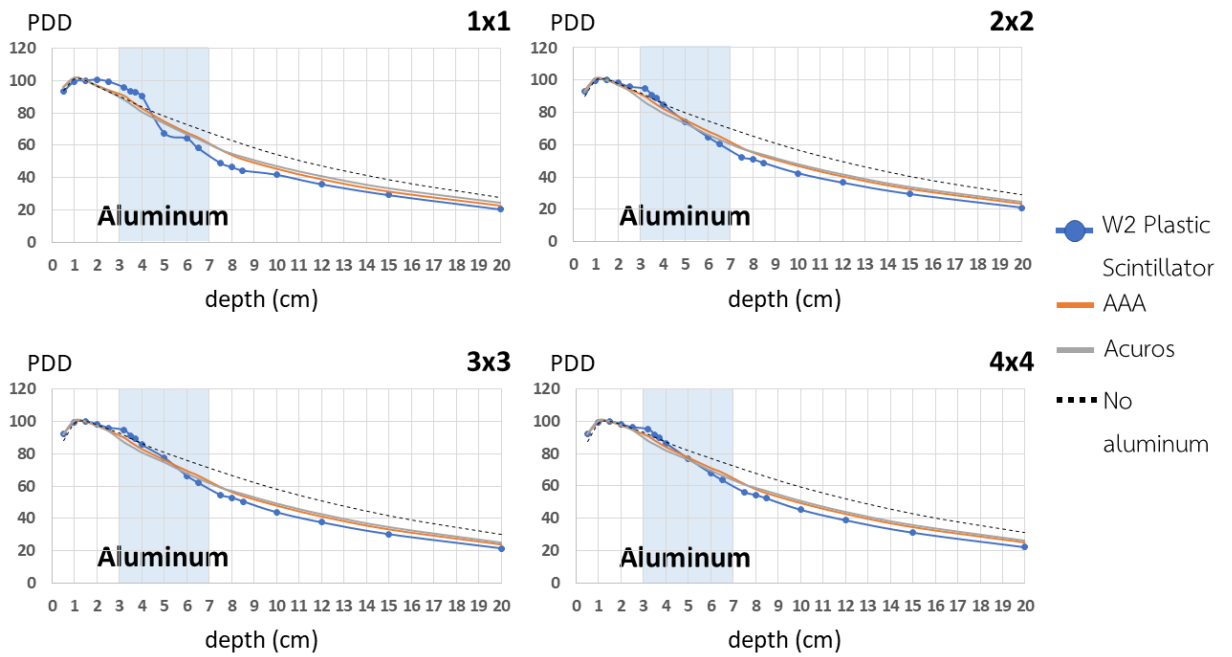


Figure 4.7 The percentage depth dose curve of 6 FFF with different field sizes in aluminum heterogeneous media

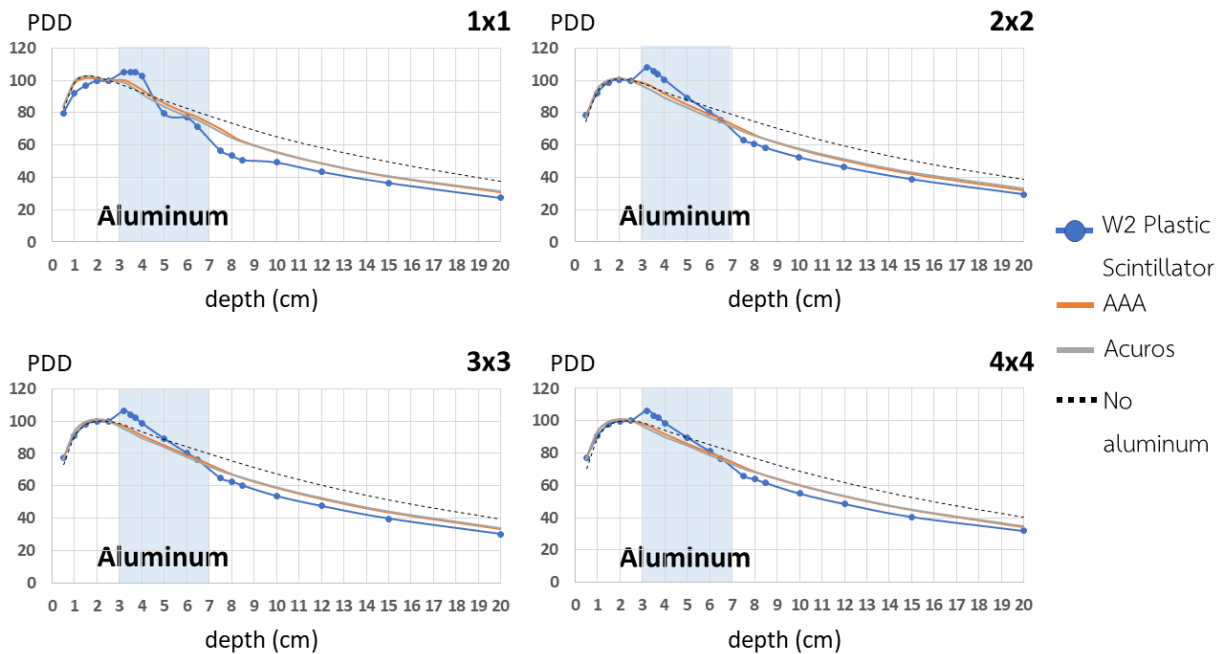
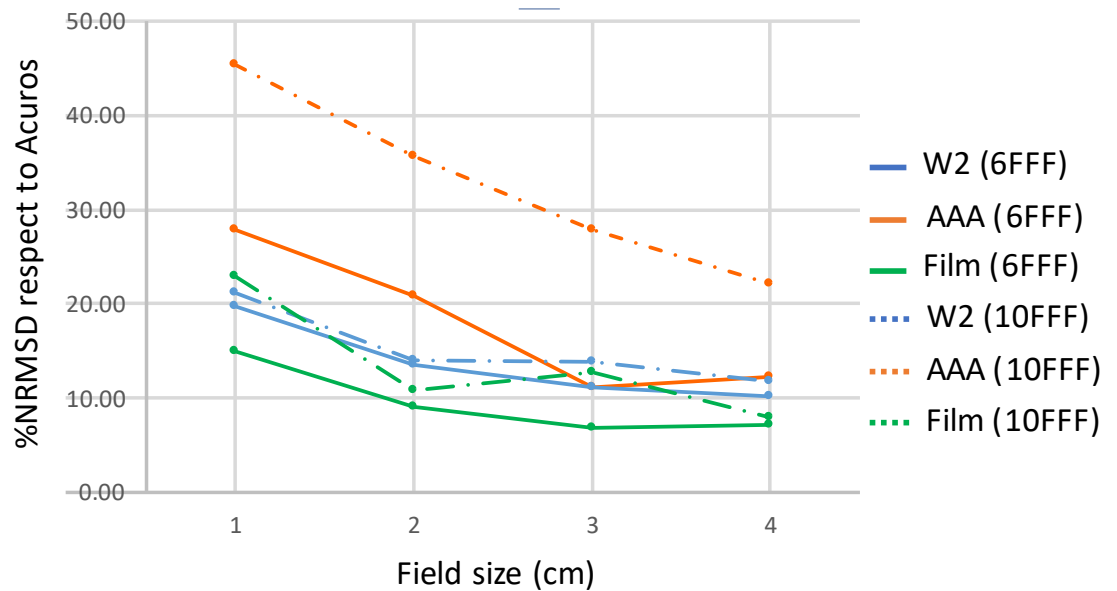
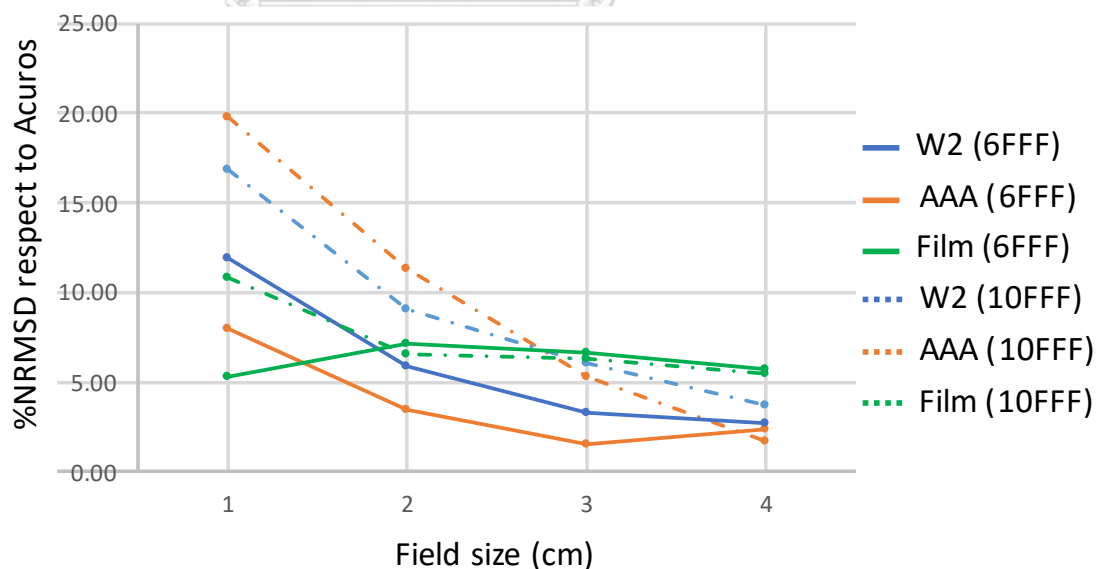


Figure 4.8 The percentage depth dose curve of 10 FFF with different field sizes in aluminum heterogeneous media

The graphical results of %NRMSD between Acuros and other percentage depth dose curves are shown in Figure 4.9 to Figure 4.11 for air, lung and aluminum inhomogeneities respectively.



**Figure 4.9** The plotted curves of %NRMSD of W2 plastic scintillator and AAA respect to Acuros for every field size in air heterogeneous media at two different energies



**Figure 4.10** The plotted curves of %NRMSD of W2 plastic scintillator and AAA respect to Acuros for every field size in lung heterogeneous media at two different energies

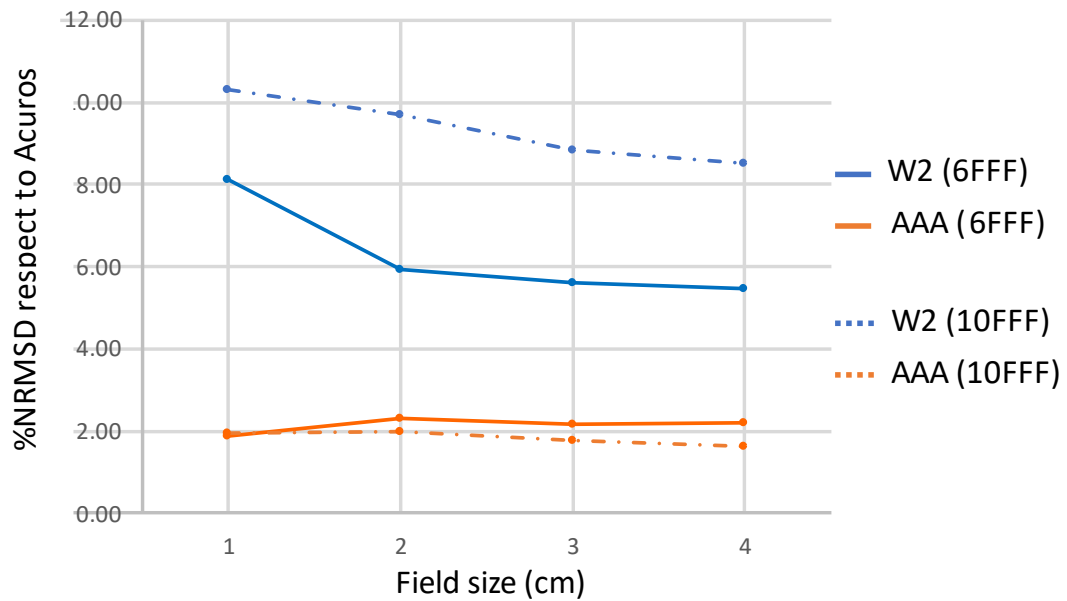


**Figure 4.11** The plotted curves of %NRMSD of W2 plastic scintillator and AAA respect to Acuros for every field size in aluminum heterogeneous media at two different energies

#### 4.2.1 Air heterogeneous media

The PDD curves of measurements and algorithms calculation are shown in Figures 4.3 and 4.4. The air heterogeneity region is presented in the shaded area. Inside air heterogeneity, the PDD curve measured by the plastic scintillator was lower than the curve that calculated by AAA, however, it was higher than Acuros curve. The %NRMSD referred to the deviation between Acuros and other PDD curves. The highest %NRMSD was found in AAA as shown in Figure 4.8. For W2 plastic scintillator, the %NRMSD deviation was between 10.1% to 19.8% for 6 FFF and between 11.8% to 21.2% for 10 FFF. The highest %NRMSD of plastic scintillator was found in 10 FFF with field size 1x1 cm<sup>2</sup>.

#### 4.2.2 Lung heterogeneous media

The %NRMSD of plastic scintillators were in the range of 2.7 – 11.9% and 3.7 – 16.9% for 6 FFF and 10 FFF respectively as shown in Figure 4.5-4.6. For 6 FFF, the AAA gives the lowest %NRMSD when compared to other curves from field sizes larger than 1x1 cm<sup>2</sup>.



### 4.2.3 Aluminum heterogeneous media

The %NRMSD of plastic scintillators were in the range of 5.48 – 8.13% and 8.52 – 10.31% for 6 FFF and 10 FFF respectively as shown in Figure 4.7-4.8. In aluminum heterogeneous media, the AAA presented the lower %NRMSD compared to the plastic scintillator for all field sizes and energy.

### 4.3 Clinical application in CIRS thorax

The result showed the percentage difference between measured and calculated dose in the CIRS thorax phantom that the average of percentage difference was 2.62% with 0.94 SD as shown in table 4.3.

**Table 4.3** The percentage difference between measured and calculated dose in CIRS thorax phantom

No.	Tumor volume (cc)	Energy (FFF)	Calculated dose (cGy)	Measured dose (cGy)	Difference (%)
1	3.5	6	1015.6	1042.8	2.67
2	9.1	6	1054.6	1077.4	3.82
3	21.5	6	1132.3	1137.8	2.12
4	50.0	6	840.4	843.23	1.97
5	73.9	6	1211.8	1209.2	-1.41
6	3.6	10	1211.5	1243.6	4.00
7	5.2	10	1025.7	1043.8	3.10
8	8.8	10	745.5	769.3	4.54
9	39.6	10	925.7	941.5	3.04
10	40.2	10	1288.7	1302.3	2.38

## CHAPTER V

### DISCUSSION AND CONCLUSION

#### 5.1 Discussion

##### 5.1.1 W2 plastic scintillator characteristics in water

The characteristics of W2 plastic scintillator is very good. The results showed that it has good linearity covering the range of 10-2000 cGy with little repetition rate and energy dependence that agree with previous W2 plastic scintillator characteristics study.<sup>(23)(24)</sup>

##### 5.1.2 Percentage depth dose in heterogeneous media

The PDD results showed the same trend in both air and lung heterogeneities that presented the dose drop in the inhomogeneity slabs and re-buildup after that. The lowest PDD of W2 plastic scintillator dropped to 40.5% for 6 FFF and 33.0% for 10 FFF in air and it dropped to 60.8% for 6 FFF and 55.7% for 10 FFF inside lung heterogeneity. In air heterogeneous media, the AAA was not accurate enough when compared with the measurement. In lung heterogeneous media, the difference between each PDD was not large as in air.

In contrast to air and lung heterogeneous media, the PDD of the plastic scintillator presents the dose buildup at interface between solid water and aluminum and dropped after that however, this effect does not present in algorithm calculation curve of Acuros and AAA. The plastic PDD showed the larger difference from Acuros when compared to AAA.

From the previous study of PDD in the heterogeneity of W1 plastic scintillator,<sup>(1)</sup> their study compared measured value to calculated data from 4 algorithms AAA, Acuros, XVMC and SP. Hence this study is unique in comparing measured and calculated values by using Acuros based on Monte Carlo simulation as a gold standard.

The calculated PDD curve from Acuros and AAA showed the same trend as in the previous study<sup>(1)</sup>, in air and lung, both W1 and W2 PDD curve were dropped inside heterogeneity region and re-buildup after that. The large difference between the plastic scintillator curve and calculation inside heterogeneous media is presented with higher energy, smaller field size and lower density medium. This effect corresponds to the previous study of W1 plastic scintillator.<sup>[1]</sup> However, the PDD of W1 presented a better agreement with Acuros PDD curve when compared to W2. This can be confirmed by the value of %NRMSD. The %NRMSD in air and lung W1 were not more than 10.0% in all field sizes and energies but for W2, %NRMSD were up to 10.1 – 21.2% and 2.7 – 16.9% in air and lung respectively. In aluminum, the dose buildup at the upper interface of aluminum and water was not founded in W1 study. The W1 PDD curve performed a very good agreement with AAA and Acuros calculation. The %NRMSD of W1 in aluminum was very low about 5.1 – 8.3% while the %NRMSD of W2 was up to 5.4 – 10.3%.

### 5.1.3 Clinical application in CIRS thorax phantom

The differences between measured and calculated doses are in the range of 1.41 – 4.54%. The smaller target trended to present the larger error that might be due to the accuracy of scintillator positioning. The larger difference was found in the high energy of 10 FFF than 6 FFF due to the longer side scattering electron range.

## 5.2 Conclusion

The W2 plastic scintillator performs very good characteristics in water in terms of short-term reproducibility, linearity, repetition rate and energy dependence with maximum deviation within 1%. The plastic scintillator PDD results show the same trend in both air and lung heterogeneity which present the dose drop in heterogeneous media region and the dose re-buildup after that. On the contrary, the

dose increases at the upper interface of aluminum and decreases after that. The large difference of plastic scintillator PDD curve inside heterogeneous media is presented with higher energy, smaller field size and lower density medium. The result of clinical application in CIRS thorax phantom shows that differences between measured and calculated doses are in the range of -1.41% to 4.54%. Hence, the W2 plastic scintillator possibly to be applied for clinical application of small-field dosimetry in heterogeneous media with the accuracy within 5% according to IAEA TRS 430.



## REFERENCES

1. Alagar AGB, Mani GK, Karunakaran K. Percentage depth dose calculation accuracy of model based algorithms in high energy photon small fields through heterogeneous media and comparison with plastic scintillator dosimetry. *Journal of applied clinical medical physics*. 2016;17(1):132-42.
2. Létourneau D, Pouliot J, Roy R. Miniature scintillating detector for small field radiation therapy. *Medical physics*. 1999;26(12):2555-61.
3. Charles P, Crowe S, Kairn T, Kenny J, Lehmann J, Lye J, et al. The effect of very small air gaps on small field dosimetry. *Physics in Medicine & Biology*. 2012;57(21):6947.
4. Morin J, Béliveau-Nadeau D, Chung E, Seuntjens J, Thériault D, Archambault L, et al. A comparative study of small field total scatter factors and dose profiles using plastic scintillation detectors and other stereotactic dosimeters: the case of the CyberKnife. *Medical physics*. 2013;40(1):011719.
5. Palmans H, Andreo P, Huq MS, Seuntjens J, Christaki KE, Meghzifene A. Dosimetry of small static fields used in external photon beam radiotherapy: summary of TRS-483, the IAEA–AAPM international Code of Practice for reference and relative dose determination. *Medical physics*. 2018;45(11):e1123-e45.
6. Aspradakis MM, Byrne J, Palmans H, Conway J, Rosser K, Warrington J, et al. Small field MV photon dosimetry: IPEM; 2010.
7. Charles P, Cranmer-Sargison G, Thwaites DI, Crowe S, Kairn T, Knight R, et al. A practical and theoretical definition of very small field size for radiotherapy output factor measurements. *Medical physics*. 2014;41(4):041707.
8. Das IJ, Ding GX, Ahnesjö A. Small fields: nonequilibrium radiation dosimetry. *Medical physics*. 2008;35(1):206-15.
9. Attix FH. *Introduction to radiological physics and radiation dosimetry*: John Wiley & Sons; 2008.
10. Papaconstadopoulos P. *On the detector response and the reconstruction of the source intensity distribution in small photon fields*: McGill University (Canada); 2016.
11. Ralston A, Liu P, Warrenner K, McKenzie D, Suchowerska N. Small field diode

correction factors derived using an air core fibre optic scintillation dosimeter and EBT2 film. *Physics in Medicine & Biology*. 2012;57(9):2587.

12. Archambault L, Beddar AS, Gingras L, Roy R, Beaulieu L. Measurement accuracy and Cerenkov removal for high performance, high spatial resolution scintillation dosimetry. *Medical physics*. 2006;33(1):128-35.

13. Scintillation Detector [Internet]. Available from:

[https://www.science.mcmaster.ca/radgrad/images/6R06CourseResources/4R6Notes4\\_ScintillationDetectors.pdf](https://www.science.mcmaster.ca/radgrad/images/6R06CourseResources/4R6Notes4_ScintillationDetectors.pdf).

14. Khan FM, Gibbons JP. *Khan's the physics of radiation therapy*: Lippincott Williams & Wilkins; 2014.

15. Xue J, McKay JD, Grimm J, Cheng CW, Berg R, Grimm SYL, et al. Small field dose measurements using plastic scintillation detector in heterogeneous media. *Medical physics*. 2017;44(7):3815-20.

16. Mani KR, Bhuiyan MA, Rahman MS, Islam SA. Open beam dosimetric characteristics of True Beam medical linear accelerator with flattening filter (WFF) and flattening filter free (FFF) beam. *Polish Journal of Medical Physics and Engineering*. 2018;24(2):79-89.

17. Plastic Scintillator [Internet]. Available from:

[https://www.standardimaging.com/uploads/files/ExradinW2\\_DS\\_1418-01.pdf](https://www.standardimaging.com/uploads/files/ExradinW2_DS_1418-01.pdf).

18. Solid Water Phantom Materials [Internet]. Available from:

[http://www.teambest.in/PDFs/dosimetry/phantoms/slabPhantoms/CNMC\\_solidwater.pdf](http://www.teambest.in/PDFs/dosimetry/phantoms/slabPhantoms/CNMC_solidwater.pdf).

19. CIRS thorax phantom [Internet]. Available from: [https://www.rpdinc.com/C-IMRT\\_Phantoms.pdf](https://www.rpdinc.com/C-IMRT_Phantoms.pdf).

20. Fogliata A, Nicolini G, Clivio A, Vanetti E, Cozzi L. Dosimetric evaluation of Acuros XB Advanced Dose Calculation algorithm in heterogeneous media. *Radiation oncology*. 2011;6(1):1-15.

21. Gagné IM, Zavgorodni S. Evaluation of the analytical anisotropic algorithm in an extreme water–lung interface phantom using Monte Carlo dose calculations. *Journal of Applied Clinical Medical Physics*. 2007;8(1):33-46.

22. Huang Z, Qiao J, Yang C, Liu M, Wang J, Han X, et al. Quality Assurance for

Small-Field VMAT SRS and Conventional-Field IMRT Using the Exradin W1 Scintillator. *Technology in Cancer Research & Treatment*. 2021;20:15330338211036542.

23. Galavis PE, Hu L, Holmes S, Das IJ. Characterization of the plastic scintillation detector Exradin W2 for small field dosimetry. *Medical physics*. 2019;46(5):2468-76.

24. Sloop AM. Characterization of the Standard Imaging Exradin W2 Scintillator Detector for Small Field Dosimetry: A Thesis. Oregon Health & Science University; 2020.



## APPENDIX

### The approval of institution review board

Certificate approval from institutional review board (IRB) of Faculty of Medicine, Chulalongkorn University, Bangkok, Thailand.



COA No. 1425/2022

IRB No. 0511/65

#### INSTITUTIONAL REVIEW BOARD

Faculty of Medicine, Chulalongkorn University

1873 Rama 4 Road, Pathumwan, Bangkok 10330, Thailand, Tel 662-256-4493

---

#### Certificate of Expedited Review Approval

(COA No. 1425/2022)

The Institutional Review Board of the Faculty of Medicine, Chulalongkorn University, Bangkok, Thailand, has approved the following study which is to be carried out in compliance with the International guidelines for human research protection as Declaration of Helsinki, The Belmont Report, CIOMS Guideline and International Conference on Harmonization in Good Clinical Practice (ICH-GCP)

<b>Study Title</b>	: Accuracy of small-field high energy photon using plastic scintillation detector in heterogenous media compared with model-based algorithm calculation
<b>Study Code</b>	: -
<b>Principal Investigator</b>	: Mr. Thanat Kaewsukri
<b>Affiliation of PI</b>	: Department of Radiology, Faculty of Medicine, Chulalongkorn University.
<b>Review Method</b>	: Expedited
<b>Continuing Report</b>	: At least once annually or submit the final report if finished.
<b>Document Reviewed</b>	:
	1. Research Proposal Version 2 Date 27/09/2022
	2. Protocol Synopsis Version 1 Date 13/06/2022
	3. Case record form Version 1 Date 13/06/2022
	4. Curriculum Vitae and GCP Training
	- Mr. Thanat Kaewsukri



All approved investigators must comply with the following conditions:

1. Strictly conduct the research as required by the protocol;
2. Use only the information sheet, consent form (and recruitment materials, if any), interview outlines and/or questionnaires bearing the Institutional Review Board's seal of approval ; and return one copy of such documents of the first subject recruited to the Institutional Review Board (IRB) for the record;
3. Report to the Institutional Review Board any serious adverse event or any changes in the research activity within five working days;
4. Provide reports to the Institutional Review Board concerning the progress of the research upon the specified period of time or when requested;
5. If the study cannot be finished within the expire date of the approval certificate, the investigator is obliged to reapply for approval at least one month before the date of expiration.
6. If the research project is completed, the researcher must send closing/final reporting the closing/final report form of the Faculty of Medicine, Chulalongkorn University.

\* A list of the Institutional Review Board members (names, positions and expertises) present at the meeting of Institutional Review Board on the date of approval of this study has been attached. All approved documents will be forwarded to the principal investigator.



- Asst.Prof. Taweap Sanghangthum, Ph.D.
- Jaruek Kanphet

Signature .....  
(Associate Professor Unnop Jaisamrarn MD, MHS)  
Vice-Chairman, Acting Chairman  
The Institutional Review Board

Signature .....  
(Associate Professor Wannarasmi Ketchart MD, PhD)  
Member and Assistant Secretary, Acting Secretary  
The Institutional Review Board

Date of Approval : October 5, 2022  
Approval Expire Date : October 4, 2023

## VITA

**NAME** Thanat Kaewsuksri

**DATE OF BIRTH** 10 Feb 1998

**PLACE OF BIRTH** Bangkok Thailand

**INSTITUTIONS ATTENDED** Bachelor of Science, Department of Physics, Faculty of Science, Chulalongkorn University, Bangkok, Thailand.

